Indian Journal of Chemical Technology
Vol. 31, January 2024, pp. 105-124
DOI: 10.56042/ijct.v31i1.7607

Design, structural and theoretical characterizations of novel Schiff base compounds: Enzymes inhibitory potential using *in vitro* and *in silico* methods

Zeineb CHORFI[1], Zakia MESSASMA[1], Djouhra AGGOUN [1]*, Selma HOUCHI[2], Chawki BENSOUICI [3], Marta FERNÁNDEZ-GARCÍA[4], Daniel LÓPEZ[4], Mostafa S. Abd El-Maksoud[5], Fatima SETIFI[6], Ali OURARI [1] & Yasmina OUENNOUGHI[1]

[1]Laboratory of Electrochemistry, Molecular Engineering and Redox Catalysis, Department of Process Engineering, Faculty of Technology, University of Ferhat Abbas, Setif 19000, Algeria

[2]Laboratory of Applied Biochemistry, Faculty of Natural and Life Sciences, University Ferhat Abbas, Setif 19000, Algeria

[3]Centre de Recherche en Biotechnologie, Ali Mendjli, Nouvelle Ville UV 03, BP E73 Constantine, Algeria

[4]Instituto de Ciencia y Tecnología de Polímeros (ICTP-CSIC), Juan de la Cierva 3, 28006 Madrid, Spain

[5]Faculty of Pharmacy, Al-Azhar University, Assiut Branch, Assiut 71524, Egypt

[6]Laboratoire de Chimie, Ingénierie Moléculaire et Nanostructures (LCIMN), Université Ferhat ABBAS Sétif-1, 19000 Sétif, Algeria

*E-mail: aggoun81@yahoo.fr, djouhra.aggoun@univ-setif.dz

Received 28 October 2022 ; accepted 24 November 2023

The aim of this paper is to further explore the enzymatic properties of two synthetic Schiff base compounds. The corresponding copper complex ($Cu^{II}(L)_2$), with its Schiff base ligand (HL) have been synthesized and their spectroscopic (IR, UV-visible., NMR (^1H, ^{13}C, Dept-135) and MS), thermogravimetric (TG/DTG), electrochemical (CV) and theoretical (Density Functional Theory) using the hybrid B3LYP/6–31 G(d,p) method) properties have been studied and well discussed. The electrochemical behaviour of $Cu^{II}(L)_2$ displays the Cu(III)/Cu(II) and Cu(II)/Cu(I) redox processes. The molecular structure of HL is confirmed by X-ray diffraction analysis. HL crystalized in the triclinic system with the space group of P-1. The morphological structures are also analyzed by X-ray powder diffraction, scanning electron microscopy with energy-dispersive X-ray spectroscopy. To improve their biological activities, inhibition of the target proteins, acetylcholinesterase (AChE), butyrylcholinesterase (BChE), Tyrosinase (TYR), and Urease enzymes are tested *in vitro* and *in silico* using molecular docking. Furthermore, their ADMET parameters are analyzed. The drug-likeness results indicate that HL followed to Lipinski's, Ghose's, Veber's, Egan's and Muegge's rules contrary to its copper complex which followed only to Veber's rule. Due to the importance of cytochrome P450s proteins for detoxification, five major CYP isoforms (CYP1A2, CYP2C19, CYP2C9, CYP2D6, and CYP3A4) are also considered during *in silico* prediction.

Keywords*:* ADMET parameters, Cu-complex, Enzymatic inhibition, Molecular docking, Schiff base compounds, Structural analysis

Introduction

The coordination chemistry of divalent metal ions, like copper complexes, is actually the subject of many studies since, these compounds were successfully explored in diverse biological systems[1]. Their properties can be improved and modified by linking to copper transition metal ion that has playing pertinent roles in diverse metabolic functions in human beings. These compounds revealed that they offer a great variety of pharmacological properties including antioxidant[2], anticancer[3], antibacterial[4], antiviral[5] and anti-inflammatory agents[6]. Adding to all of these properties, in drug discovery, the inhibition of key enzymes is one of the most reliable strategies. It could alleviate observed symptoms in a variety of pathologies[7].

First, Tyrosinase is therapeutic target validated for the treatment of skin pigmentation[8]. Indeed, this enzyme participates in the regulation of the first two steps of the melanogenesis process[9,10]. The elevation of synthesis and accumulation melanins in the skin is a common feature in many types skin disorders[11]. Thus, the inhibition of TYR would serve to decrease the level melanins and to design and develop new depigmenting compounds useful in pharmaceutical and cosmetic area for the treatment of skin blemishes. Then, cholinesterase enzymes play an important role in the development of Alzheimer's disease. They are a family of enzymes that catalyze the hydrolysis of acetylcholine (ACh) neurotransmitter to choline and acetic acid[12]. ACh is one of the neurotransmitters most closely involved in memory storage,

consolidation and recall functions. It is a chemical messenger key used by neurons to transmit signals to each other that subscribe to cognitive processing as well as basic thoughts. Several studies have shown low levels of acetylcholine in patients with Alzheimer's disease[13]. Acetylcholinesterase (AChE) inhibition undoubtedly contributes to the improvement of ACh levels, thus alleviating the symptoms associated with Alzheimer's disease.

Furthermore, Urease is an enzyme that catalyzes hydrolysis of urea to ammonia and carbamate, which is the final step of nitrogen metabolism in living organisms. It is widely distributed in a variety of fungi, plant and bacteria such as *Helicobacter pylori* and *Proteus mirabilis*. It has been reported that urease has adverse effects on agriculture, stockbreeding and human[14]. The high and uncontrolled activity of urease results in excessive ammonia release and increased pH of the environment, bringing about damaging consequences in human and agriculture, such as gastrointestinal infections and destruction of plant roots[15]. It is the major cause of pathologies induced by Helicobacter pylori (*H. pylori*) that permits to the bacteria to live in the acidic environment of stomach[16] and was a major cause of peptic ulcers. So, anti-ulcer drugs focused on urease inhibitor remains the center of interest for many researchers.

The field of the application of the complexes towards the therapy or diagnosis of diseases is a relatively young discipline and the introduction of these complexes in pharmaceutical remedies has been supported. Therefore, in continuation of our recent works[17-19], our efforts have been intensively oriented on the synthesis, the spectral characterization (IR, UV-visible., NMR, MS), the electrochemical (CV), thermal (TG and DTG) as well as powder XRD, SEM and EDX characterizations of these compounds (Scheme 1). The structure of the ligand was determined by X-ray crystallography. Furthermore, systematic theoretical studies on these prepared compounds have also been carried out by DFT investigations attempting to study and confirming the hypothetical molecular structures previously obtained. Finally, four enzymes (acetylcholinesterase (AChE), butyrylcholinesterase (BChE), Tyrosinase (TYR), and Urease) were used as the target proteins, *in vitro* and *in silico* by using molecular docking of both the synthesized compounds.

Experimental Section

Materials and methods

All chemicals and solvents were obtained from commercial sources (Sigma Aldrich) and were used as received. The molar conductivities of DMSO solutions ($5\cdot\times10^{-4}$ M) were measured by using Meterlab CDM210 conductivity-meter instrument. Infrared spectra were obtained using a Perkin-Elmer 1000 IR spectroscopy instrument. A Unicam UV-300 Spectrophotometer was used to acquire the Ultraviolet (UV)-visible spectra. The microanalysis was achieved for C, H, and N using a Carlo Erba EA1108 elemental analyzer.NMR (^{1}H, ^{13}C and DEPT 135) spectra using deuterated DMSO were recorded on a 500 MHz Bruker-Avance III NMR spectrometer at 25°C. High-resolution mass spectra were recorded by electrospray ionization-mass spectrometry (ESI-MS) with the aid of a Bruker APEX-2 instrument in ESI-grade acetonitrile solvent. Thermal characterization was performed on a TA Instruments

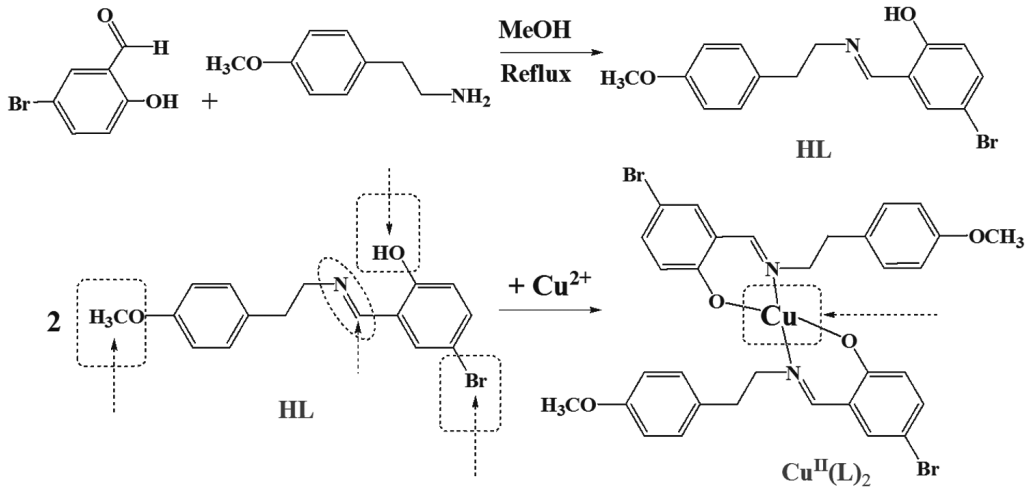

Scheme 1 — Reaction ways leading to the formation of HL and its copper complex $Cu^{II}(L)_2$

TGA Q500 thermal analyzer in dynamic mode under nitrogen atmosphere (Flow rate 60 mL min^{-1}). Under heating rate of 10 °C min^{-1}, samples were heated from room temperature to 900°C. SEM samples images were obtained using a Hitachi SU8000 microscope operating at 200 kV.For the X-ray powder diffraction spectroscopy (XRD), the diffractograms were recorded between 4° and 90° in an X-ray diffractometer model Rigaku Ultima IV with a 2θ step size of 0.02° and a step time of 10 s, Cu tube wavelength of 1.54 Å and graphite monochromator40 kV voltage and 20 mA generator current. Cyclic voltammograms were recorded in 0.1 M tetrabutylammonim perchlorate(TBAP) solution as electrolyte were supported using a 301/10 Potentiostat/Galvanostat type PGZ 301-VoltaLab 10 radiometer with a glassy carbon (GC), a saturated calomel electrode (SCE) and a platinum wire as working, reference and auxiliary electrodes.

Chemistry

Synthesis of the Schiff base ligand (noted HL)

To a methanolic solution of p-methoxy phenylethylamine[$C_9H_{13}NO$] (0.152 g, 1 mmol, 10 mL), slowly was added a methanolic solution of 5-bromo-2-hydroxybenzaldehyde [$C_7H_5BrO_2$] (0.201 g, 1 mmol, 10 mL). This mixture was maintained in reflux for three hours and then cooled to room temperature. The final desired ligand (HL) obtained after three hours of reflux was collected by filtration and washed with methanol and diethyl ether. The expected yellow crystals of HL [$C_{16}H_{16}BrNO_2$] were obtained after recrystallisation in methanol with a final yield of 81%.

Synthesis of copper Schiff base complex (noted $Cu^{II}(L)_2$)

150 mg (0.75 mmol) of methanolic solution of $Cu(CH_3COO)_2{\cdot}H_2O$ was added to 486 mg (1.5 mmol) of above synthesized Ligand corresponding to 1:2 molar ratio. After four hours under reflux, the obtained precipitate was copiously washed with methanol to obtain the pure complex with 58% as an acceptable yield.

Crystallography

Single crystals of the prepared ligands were grown by slow evaporation of methanol solvent at room temperature. It was selected and mounted on a MiTeGen loop with grease and examined on a Bruker D8-VENTURE diffractometer equipped with a Photon II CCD area detector using graphite-monochromated Mo-Kα radiation (λ = 0.71073 Å). Data were collected at 170 (2) K with APEX-III software[20], integrated using SAINT[21], and corrected for absorption using a multi scan approach (SADABS)[22] Final cell constants were determined from a full least-squares refinement of all the observed reflections. The resulting set of (h k l) was used for structure solution and refinement. The structure was solved by direct methods with SIR 2002[23], to locate all the non-H atoms which were refined anisotropically with SHELXL-2014 (Ref.24) by full-matrix least-squares on F^2 procedure within WINGX[25] suite of software used to prepare the material for publication. H-atoms were added at the calculated positions and refined with a riding model. The Mercury 3.8 (Ref.26) for Windows program was used for generating figures of the structure.

Theoretical calculations

All computations were performed by means of standard DFT method using the Gaussian 09 program package[27,28]. GaussView 05 program[29] were used to visualize the molecular structure. The geometries of HLand $Cu^{II}(L)_2$ were optimized with the B3LYP/6-31G(d,p) basis set[30]. The geometry optimizations were completed in the absence of solvent molecules and the optimized structure of HL was compared with the crystalline structure. Frontier molecular orbitals (HOMO, LUMO), band gap, molecular electrostatic potential (MEP), Mulliken atomic charge of these compounds were also computed.

Enzymatic inhibitory activities

***In vitro* inhibition assays**

A spectrophotometric method developed by Ellman *et al*. was used to determine the AChE and BChE inhibitory activities[31]. Then, the inhibitory effect of Tyrosinase was measured spectrophotometrically by the method described by Chan *et al*. and by using L-DOPA as substrate[32]. In the urease enzymatic activity, the urease inhibitory was analyzed by measuring ammonia production via the indophenol method, as described by Weatherburn[33].

Statistical analysis

All data on activity tests were the averages of triplicate analyses. The data were recorded as means ± standard error meaning. Significant differences between means were determined; p values <0.05 were regarded as significant.

***In silico* molecular docking studies**

Molecular docking was performed to predict the maximum binding affinity between the ligands and

the crystal structures of targeted proteins using AutoDock vina. Also, BIOVIA discovery studio was used to find the types of interactions with different amino acid residues[34]. We perform re-docking for the co-crystalized ligands and 3D crystal structures of the protein to validate the previously mentioned softwares. The drug-protein interactions of HL and $Cu^{II}(L)_2$with Human acetylcholinesterase (PDB ID: 4EY7)[35], Human butyrylcholinesterase (PDB ID: 4TPK)[36], Mushroom tyrosinase (PDB ID: 2Y9X)[37], and Helicobacter pylori urease (PDB ID: 1E9Z)[38] were analyzed by *in silico* molecular docking technique. The 3D structures of the proteins were retrieved from Protein Data Bank in RSCB (Research Collaboratory for Structural Bioinformatics) website in PDB format. The 2D structures of the ligands were sketched using Chamedraw ultra (v12.0). Ligands and proteins were fully optimized for docking using AutoDock tools (ADT) v1.5.6 packages[39]. These optimizations include removing water molecules, addition of hydrogens, addition of the charges, and adjusting the grid box configuration to the most functional active site. It also, includes removing the co-crystalized ligands for preventing unwanted interactions during docking.

ADMET prediction

The pharmacokinetic assessment of the structures of HLand its $Cu^{II}(L)_2$was performed through the freely available online SwissADME web tool (http://swissadme.ch/index.php)[40,41]. While, toxicity predictions were assessed using the pkCSM server (http://biosig.unimelb.edu.au/pkcsm/prediction, accessed on August 10th, 2022)[42].

Results and Discussion

Synthesis and physicochemical properties of the synthesized compounds

The structures of bidentate NO ligand with its neutral copper(II) complex are shown in Scheme 1. Their analytical data and some physical characteristics are described in Table 1. The molar conductance measurements are very small which can be explained by their non-electrolytic nature at room temperature[43]. The measured melting temperatures improve the stability of the prepared compounds. Characterization was performed by CHN elemental analysis confirming the proposed structures. As it can be seen, we have found that the theoretical values are in a good agreement with the obtained experimental values. IR, UV–visible, NMR, MS, TG/DTG, powder XRD, SEM/EDX and cyclic voltammetry techniques were also studied. The structure of HL was also confirmed by X-ray crystallographic study.

Spectral characterization

Infrared spectra

The main IR spectra of HL and $Cu^{II}(L)_2$ complexin the 400–4000 cm^{-1} region are shown in Fig. S1. The spectrum of HL shows a weak broad band at 3459 cm^{-1} assignable to the intra-molecular hydrogen bonded –OH group. In the both spectra, the bands appear around 2914–2923 cm^{-1} correspond to the aliphatic and aromatic elongation vibration (C-H)[18]. The characteristic C=N stretches at 1633 cm^{-1} for HL[44], which undergoes a slight bathocromic displacement of about 10 cm^{-1} for $Cu^{II}(L)_2$ complex. This result confirms the participation of nitrogen atoms of the both azomethine functions in the coordination of copper ion[45]. In addition, the strong phenolic (Ar–O) stretch situated at 1370 cm^{-1} (Ref.29) in the ligand spectrum, has undergone a hypsocromic displacement with an average of 15 cm^{-1}. This band moves to 1389 cm^{-1} in the copper complex spectrum which confirms that the oxygen atom of this (C-O) group is effectively bonded to the metal ions[44]. The presence of an absorption band at around 824 cm^{-1} corresponds to the vibrations of the C-Br bond[46]. The far detected new bands in infrared spectrum of the copper complex, observed around 470–458 cm^{-1} and 650–698 cm^{-1}, may be attributable to the frequencies that are probably due to the formation of Cu–N and Cu–O bands, respectively[47,18]. Harmonic vibrational frequencies of HL and $Cu^{II}(L)_2$were computed using the DFT/B3LYP method with the 6-31G (d,p) basis

Table 1 — Physical and analytical data of HL and its copper complex

Sample	Mol. wt. (g/mol)	Colour	Yield (%)	Frontal report (Rf)	Melting point (°C)	Molar conductivity (μs/cm)	Elemental Analysis Obt. (Calc.) %		
							C	H	N
HL	334.02	Yellow	81	0.80	185	3.37	57.38	4.73	4.38
$C_{16}H_{16}NO_2Br$		Crystal					(57.48)	(4.83)	(4.19)
$Cu^{II}(L)_2$		Olive	58	0.66	230	4.63	52.50	4.06	4.07
$C_{32}H_{30}N_2O_4Br_2Cu$	729.57	Powder					(52.63)	(4.14)	(3.84)

set. As presented in Table S1 and Fig. S1, it can be seen that the experimental values have a better correlation with the corresponding calculation values. This confirms the validities of the optimized structures of the studied compounds.

Electronic absorption spectra

Electronic spectra of HL were recorded in the range 200-800 nm with some least and most polar solventswith a concentration of $1.0 \cdot 10^{-5}$ M as illustrated in Fig. S2. In UV-visible spectra, the key factor which influences the maximum absorption wavelengths changes is the polarity of the medium that can cause generally several changes in the intensities, shapes and positions of the absorption bands[48]. These spectral changes are probably attributed to the presence of hydrogen bonding interaction formed between solute-solvent and/or solute-solute[49,50].

According to Fig. S2a, changing the solvent from MeOH to DMF causes some different shifts to the bands attributed to n-π* (around 320 nm) and π-π* (around 270 nm). Slight blue shifts (bathochromic effect) for these bands were clearly noted[51]. The absorption spectrum of $Cu^{II}(L)_2$ (Fig. S2b) exhibited two bands around 260–310 nm. These bands are assigned to intra-ligand transitions (π-π* at 270 nm and n-π* at 302 nm)[51]. The spectrum showed also a third band at 380 nm which may be ascribed to ligand-to-metal charge transfer (LMCT) transitions[52]. Furthermore as shown in Table S2 and Fig. S2, TD-DFT calculations based on the B3LYP/6-31G(d. p) level for the optimized geometry are in a good agreement with the experiment results aforementioned.

Nuclear magnetic resonance (^1H, ^{13}C and DEPT-135) spectra

HL was also characterized by ^{1}H-NMR, ^{13}C-NMR and DEPT-135 spectroscopic methods and its spectra have been recorded DMSO as deuterated solvent (Fig. S3). The ^{1}H NMR spectrum displayed a singlet signal at 13.616 ppm which is attributed to the phenolic OH resonances of HL. The signal appearing at δ = 8.411 ppm corresponds to the H-C=N-azomethinic proton. The aromatic protons resonate in the range of δ=7.726–6.657 ppm. The protons of methoxy group (δOCH_3) attached to the aromatic ring are also observed as singlet at δ= 3.730 ppm. The peak observed at δ= 2.459 ppm was assigned to the solvent peak (DMSO). The both triplet peaks appearing at δ = 2.842 ppm and δ = 3.766 ppm correspond to the Ph-CH_2 and N-CH_2 methylene protons, respectively. The ^{13}C NMR spectrum is consistent with number of carbons in its structure and it shows 14 signals (Fig. S3). The imine carbon (>C=N) appears at 165.201 ppm. The aliphatic Ph–CH_2, N–CH_2, and –OCH_3carbon peaks are detected at 36.036, 60.093, 55.429 ppm, respectively. The aromatics carbons are observed in the expected region between 109 and 160 ppm. Further complete assignments of all carbons and some structural precisions were perfectly elucidated by recording ^{13}C DEPT 135 experiments. DEPT 135 spectrum gave information on the methylene carbon (CH_2) which appeared as the negative signal while the methine (CH) and methyl (CH_3) carbon appear as positive signals. So, as it can be seen in the DEPT 135 spectrum, two methylene carbons of the ethyl chain showed negative signals at 36.034 ppm and 60.093 ppm. The signal at δ 55.428 ppm appeared in the positive region of DEPT 135 spectrum, confirming that this carbon signal belongs to the methyl carbon. Therefore, the obtained results support the structure of HL and are in perfect agreement with those reported in the literature[53,54].

Mass spectra

The mass spectra of HL and $Cu^{II}(L)_2$were performed and investigated as shown in Fig. S4. The both spectra show original molecular weight, which are in good agreement with the expected values corroborate with their formula weights. The mass spectrum of HL gives a peak at ~135 m/z, which is assigned to the molecular ion $[C_9H_{11}O]^+$ methoxyphenylethyl peak. The peak given at ~334 m/z, is ascribed to molecular ion peak of $[HL]^+$. The mass spectrum of Cu(II) complex gives a peak at ~730 m/z attributed to the monoprotonated of the parent peak $[Cu^{II}(L)_2+H]^+$ and gives also a molecular ion peak at ~752 m/z, assigned to $[Cu^{II}(L)_2+Na]^+$ peak. These results are in good accordance to the proposed structures of HL confirming as well the stoichiometry of the copper chelates according our copper complex $Cu^{II}(L)_2$.

Thermal (TG/DTG) characterization

The thermal stability was studied by controlling heating rates 10°C per minute under nitrogen atmosphere. The thermal analysis curves (TG) and their derivatives (DTG) are shown in Fig. S5. Thermograms of the samples are stable up to 200°C, designates the absence of water lattice (loses at low temperature region <120 °C) in addition to the neat absence of coordinated water (loses between 120 and 220 °C). Fig. S5a is displayed the TG/DTG

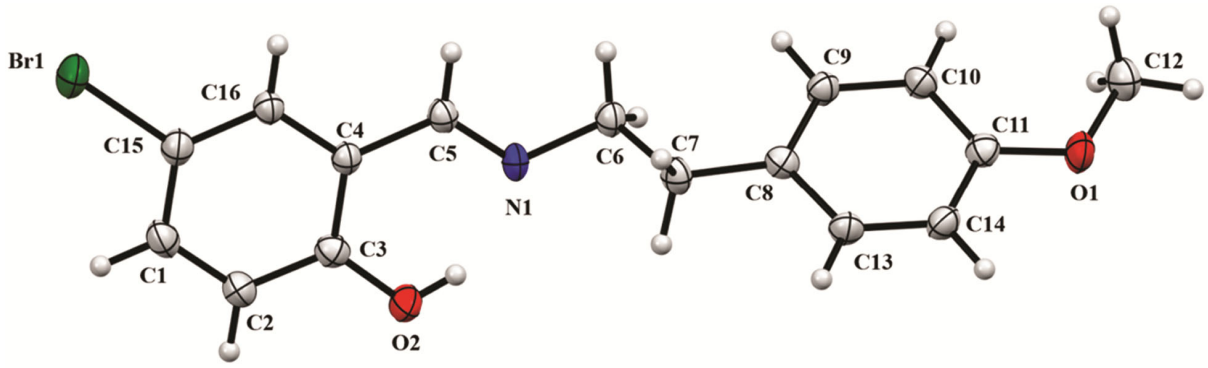

Fig.1 — The molecular geometry of compound HL. Displacement ellipsoids are drawn at the 50% probability level. H atoms are represented as small spheres of arbitrary radius

thermograms of HL, which degrades in only one step. The experimental total mass loss is about 98%, this reinforced the high purity of HL. The thermal analysis of the copper complex occurs in three decomposition steps (Fig. S5b**)**. The first decomposition around the temperature range of 250–295°C, with a weight loss of 29.47% (Theo. 29.36%) is attributed to the loss of two molecules of methoxyphenyl (2 MeOPh). The second decomposition of 23.15% (Theo. 23.43%) weight loss, obtained in the temperature range of 295–425°C, corresponds to the partial loss of the ethyl moiety with bromophenyl molecule of the organic Schiff base ligand. Finally, the third decomposition step takes place around the temperature range of 425–700 °C, which is due to the loss of the remaining organic ligand and copper oxide formation (CuO) polluted with carbon (4C) atoms as residue[55].

Crystallographic characterization

Good quality of single crystals of HL were obtained by a simple slow evaporation of a saturated methanol solution of this compound. A perspective view of the studied ligand with the selective atom numbering scheme is shown in Fig. 1. Structure refinement details, crystal data and data collection are summarized in Table 2. Some selected bond distances, angles and hydrogen-bond are listed in Tables 3 and 4, Structure determination reveals that HL crystallizes in the triclinic space group *P–1*. As shown in Fig. 1, the ligand acts as a bidentate NO through the imine nitrogen atom, N(1) and deprotonated hydroxyl group $O(2)^{-}$. The bond distances and angles are in good agreement compared with previously reported studies with similar Schiff bases ligands[56,57]. As it can be seen in Table 3, the obtained angles are slightly deviated from the ideal values of 120° (for sp^2hybridization) and 109.5 (for sp^3 hybridization).

Table 2 — Crystallographic data and structural refinement details of HL

Molecular formula	$C_{16}H_{16}BrNO_2$
Molecular weight	333.20 g mol^{-1}
Temperature (K)	170
Radiation λ (Å)	0.71073
Crystal system	Triclinic
Space group	*P-1*
a/Å	5.8371 (3)
b/ Å	7.7428 (3)
c/ Å	16.1066 (7)
α/ °	81.940 (1)
β/ °	89.619 (2)
γ/ °	85.409 (2)
V/$Å^3$	718.43 (6)
Z	2
Calculated density (mg cm^{-3})	1.545
Absorption coefficient (mm^{-1})	2.861
F(0 0 0)	338
Reflections measured/independent	37874/4406[R(int) = 0.022]
Range/indices (h, k, l)	***h***= −8→8, ***k*** = −10→11, ***l*** =
Theta range for data collection (°)	−22→23
Completeness to theta = 25.242	2.6 to 30.7
Refinement method	99.5 %
Data / restraints / parameters	Full-matrix least-squares on F^2
Goodness of fit on F^2	4406 / 0 / 182
Final R indices [I>2sigma(I)]	1.10
Extinction coefficient	R1 = 0.024, wR2 = 0.07
Largest diff. peak and hole (e.A^{-3})	n/a
	0.65 and -0.56

R = {Σ[w(|F0| - |Fc|)]/ Σ w(|F0|)}, Rw = {Σ[w(|F0| - |Fc|)^2]/Σ w(|F0|^2)}$^{1/2}$,
wR2 = {Σ[w($F0^2$ – Fc^2)^2]/ Σ w($F0^2$)}$^{1/2}$
$w = 1/[\sigma^2(F_o^2) + (0.0336P)^2 + 0.2893P]$ where $P = (F_o^2 + 2F_c^2)/3$

The hydrogen atom H(1), attached to the carbon atom C(1), is involved in an C–H…A interaction within the $Br1^{i}$ with the related symmetry ((i) −x, −y, −z).

Quantum chemical calculations

Optimized structure

In gas phase, B3LYP functional with 6-31G(d,p) basis sets as incorporated in the Gaussian 09W

Table 3 — Bond lengths and angles in HL structure (Å, °)

Br1—C15	1.8954 (13)	C11—O1—C12	117.63 (11)	N1—C5—H11	119.9
O1—C11	1.3673 (15)	C5—N1—C6	119.99 (11)	N1—C6—C7	109.11 (10)
O1—C12	1.4279 (17)	O2—C3—C2	118.85 (11)	N1—C6—H13	109.9
O2—C3	1.3474 (16)	O2—C3—C4	121.44 (11)	N1—C6—H12	109.9
N1—C5	1.2781 (16)	O1—C11—C10	125.21 (11)	C16—C15—Br1	118.66 (9)
N1—C6	1.4600 (15)	O1—C11—C14	115.22 (11)	C1—C15—Br1	120.26 (9)
		N1—C5—C4	120.30 (11)		

Table 4 — Hydrogen bonds for shelx_x [Å and deg.]

D—H···A	D—H	H···A	D···A	D—H···A
C1—H1···Br1i	0.95	3.13	3.9908 (13)	151

Symmetry code for HL Schiff base ligand: (i) −x, −y, −z with D = donor; H = hydrogen; A = acceptor

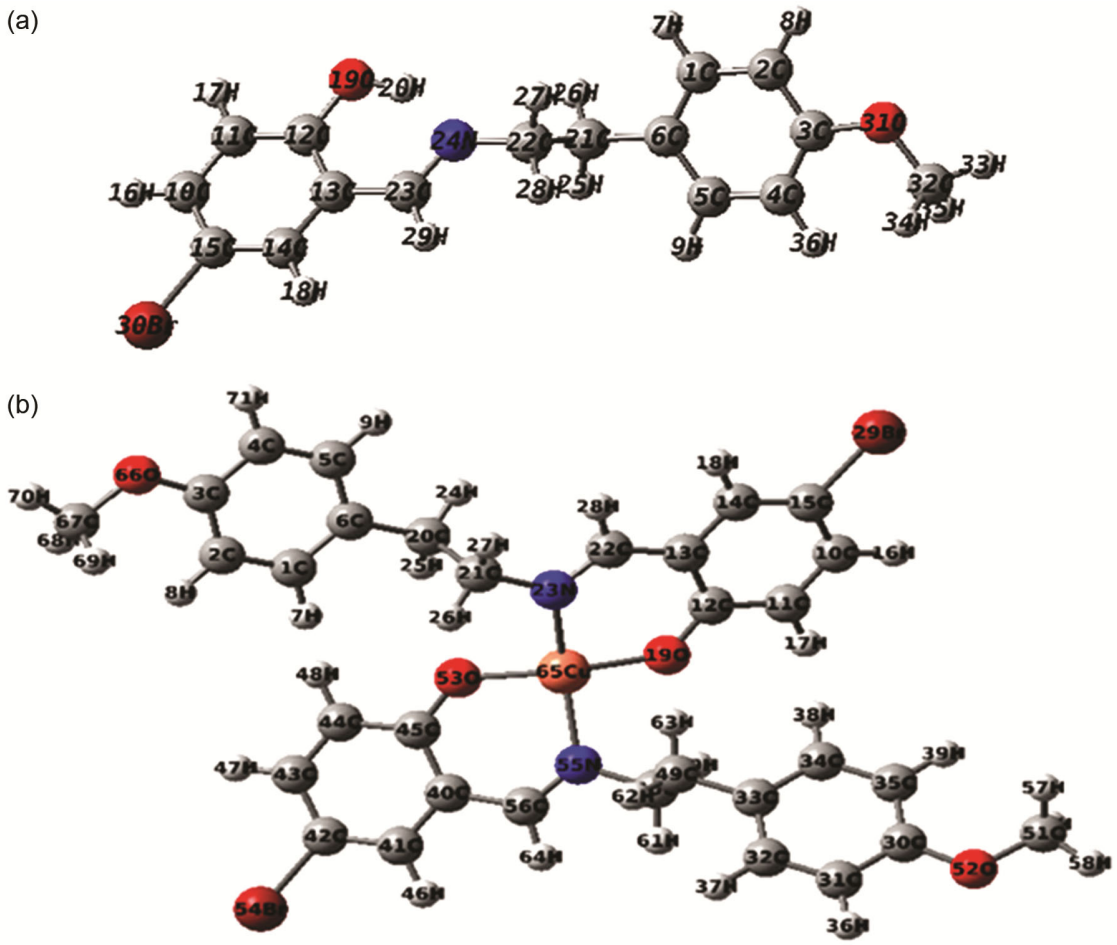

Fig. 2 — Optimized structures of (a) HL and (b) $Cu^{II}(L)_2$with the numbering of atoms computed from the B3LYP/6-31G (d,p) method

program is used to prepare the geometry optimization of the samples. These optimized geometries are shown in Fig. 2, while the experimental and calculated bond lengths and bond angles of HL are summarized in Table 5. It can be easily seen from this Table that utmost of the calculated bond lengths and bond angles matched with the experimental values. It is noted that theoretical structure is related to the isolated molecule without intermolecular interactions with the neighboring molecules, whereas, the experimental results are associated to interacting molecules in the crystal lattice[58]. The C5=N1 and O2-C3 bond lengths are1.2781 (I6) and 1.3474 (16) Å in X-ray structure, whereas the calculated values are 1.2936 and 1.38 Å in optimized geometry, respectively. These values are in good agreement with

Table 5 — The calculated and experimental values of the bond lengths and bond angles of HL

Bond lengths (Å)	X-ray	B3LYP	Bond angle (°)	X-ray	B3LYP	Bond angles (°)	X-ray	B3LYP
Br1-C15	1.8954	1.91	C11-O1-C12	117.63	120.0	N1-C5-H11	119.9	109.4712
O1-C11	1.3673	1.43	C5-N1-C6	119.99	120.0	N1-C6-C7	109.11	109.4712
O1-C12	1.4279	1.43	O2-C3-C2	118.85	120.0	N1-C6-H13	109.9	109.4712
O2-C3	1.3474	1.38	O2-C3-C4	121.44	120.0	N1-C6-H12	109.9	120.0
N1-C5	1.2781	1.2936	O1-C11-C10	125.21	120.0	C16-C15-Br1	118.66	120.0
N1-C6	1.4600	1.47	O1-C11-C14	115.22	120.0	C1-C15-Br1	120.26	120.0

Table 6 — Some important bond lengths (Å) and angles (°) of $Cu^{II}(L)_2$ complex

Bond length (Å)					
C1-C6	1.4737	C22-N23	1.2696	Cu65-O53	1.8095
C1-H7	1.0702	N55-C56	1.274	Cu65-N55	2.734
C5-C6	1.4001	N23-Cu65	2.7354	Br29-C15	1.9098
C6-C20	1.5402	C12-C13	1.4875	O66-C3	1.431
C20-C21	1.5395	C22-C13	1.5826	O66-C67	1.4312
C21-H26	1.0694	C12-O19	1.4811	C67-H68	1.0693
C21-N23	1.4694	O19-Cu65	1.8161	C67-H69	1.0693
Bond angle (°)					
C21-N23-Cu65	122.8953	C22-C13-C12	131.3625	N55-Cu65-O19	117.3098
H27-C21-N23	109.6764	C13-C12-O19	132.3388	Br29-C15-C10	119.9017
C22-N23-Cu65	122.8951	N23-Cu65-O19	97.1427	O66-C67-H68	109.337
C22-N23-H28	118.4065	N55-Cu65-O55	95.49	C40-C45- O53	131.3644
C22-C13-H28	118.4065	N23-Cu65-O53	116.179	C50-N55-Cu65	123.9532

the corresponding values in the similar Schiff base[59]. The biggest difference of calculated and experimental bond lengths is observed at O1-C11 bond, with the different value being 0.06 Å. For the bond angles, the largest difference occurs at C11-O1-C12 bond angle, with the different value being 2.3º(See Fig. S6**)**. Hence, the theoretical calculation results in a very good approximation and as a result of this it could be very useful to calculate the other parameters. A square planar geometry is formed between HL and copper ions through coordination via nitrogen and phenolic oxygen. Both phenolic OH groups are deprotonated. The nitrogen atoms are at trans position to oxygen atoms. The trans N-Cu-O angles are about 96° and the cis angles about the central Cu atom between 116.017 and 117.30°, which indicate a distorted square planar geometry. As expected, there was a small change in the geometric arrangement of the structures of HL and its complex. Some selected optimized values of bond lengths and angles of $Cu^{II}(L)_2$obtained from DFT calculations are listed in Table 6. We observed an increase in the bond length distances around the coordinating atoms to the Cu atom of the complex; the C-O bond lengths in the complex are significantly longer than that in the ligand as the result of the deprotonation of the phenolic groups. On the other hand, the N=C (azomethine) bond lengths are slightly shorter than that in the ligand. Other bond lengths and angles are in normal ranges and comparable with those reported in literature[60].

Frontier molecular orbital analysis (FMO)

Frontier molecular orbitals (FMO) have an important role for determination of chemical reactivity of compounds. HOMO largely acts as an electron donor while LUMO acts as an electron acceptor. The gap between HOMO and LUMO determines molecular chemical stability. Compounds with higher energy gap have a lower chemical reactivity[61]. The distributions and energy levels of the HOMO and LUMO orbitals of HL and $Cu^{II}(L)_2$ complex are shown in Fig. 3. As it is shown, the positive region is presented in red and the negative one in green to further determine the relationship between delocalization and reactivity, global descriptors were applied. The reactivity parameters were calculated according to the approximations of energies E_{HOMO} and E_{LUMO} states, based on the optimization of the fundamental state geometry. The calculated parameters, energy gap (E_{gap}), ionization potential (I), electronic affinity (EA), chemical potential (μ), electronegativity (χ), chemical hardness (η) and electrophilicity indices (ω) are collected in Table 7, in which is observed that the complex of copper $Cu^{II}(L)_2$ presents a higher capacity to form anions due to the electronegativity value (χ), which

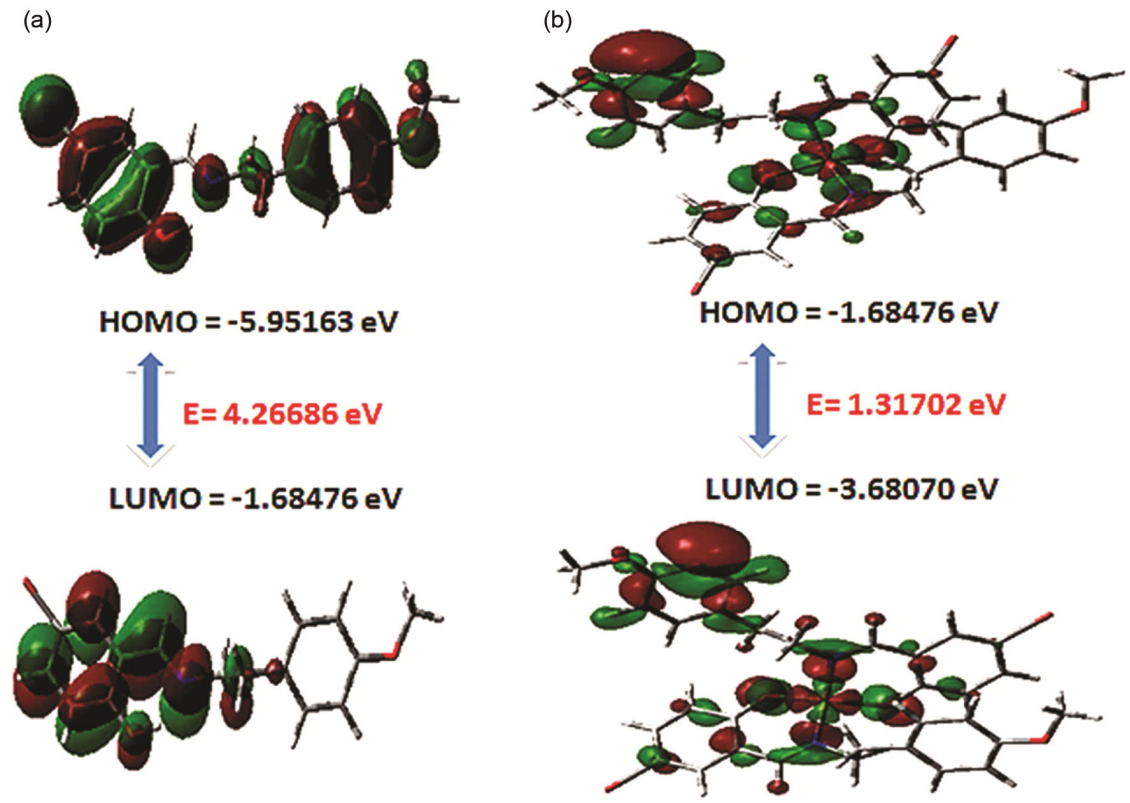

Fig. 3 — Presentation of the energy levels, energy gaps, and frontier molecular orbitals of (a) HL and (b) $Cu^{II}(L)_2$

Table 7 — Global chemical reactivity parameters calculated in eV at the B3LYP/6–31G(d,p) level of theory

Compound	HOMO	LUMO	Egap	IP	EA	μ	χ	η	ω
HL	-5.95163	-1.68476	4.26686	5.95163	1.68476	-3.8180	3.8180	2.13329	3.12419
$Cu^{II}(L)_2$	-4.99718	-3.68070	1.31702	4.99718	3.68070	-4.33894	4.33894	0.65824	14.3005

$\Delta E = E_{HOMO}-E_{LUMO}$, $IP = -E_{HOMO}$, $EA = -E_{LUMO}$, $\mu = (E_{HOMO} + E_{LUMO})/2$, $\chi = -(E_{LUMO}+E_{HOMO})/2$, $\eta = (E_{LUMO}-E_{HOMO})/2$, $\omega = \mu^2/2\eta$

represents a greater tendency to attract electrons. Chemical hardness is associated to the stability and reactivity of a chemical system. According to FMO, chemical hardness corresponds to the energy gap between HOMO and LUMO. As the energy gap increases, the molecule becomes harder and more stable/less reactive[62,63]. The values of electronic chemical HL and its complex of copper are presented in Table 7, where the greater electronic chemical potential (absolute values) indicates the less stable and more reactive. The electrophilicity ($\boldsymbol{\omega}$) index has become a powerful tool for the study of the reactivity of organic molecules participating in polar reactions[64]. It measures the tolerance of a species to accept electrons. A good electrophile is characterized by a high value of $\boldsymbol{\omega}$ but, in the opposite case, a good and more reactive nucleophile is rather characterized by a $\boldsymbol{\omega}$ low value. So, the electrophilicity ($\boldsymbol{\omega}$) scale allowed the classification of organic molecules as strong electrophiles with $\boldsymbol{\omega}$ >1.5 eV, moderate electrophiles with 0.8 <$\boldsymbol{\omega}$<1.5 eV and marginal electrophiles with $\boldsymbol{\omega}$ <0.8 eV[65]. Table 7 indicates that the complex $Cu^{II}(L)_2$ is stronger electrophilic with $\boldsymbol{\omega}$ > 1.5 eV. The value of ($\boldsymbol{\omega}$) for HL and $Cu^{II}(L)_2$ are 3.12419 and 14.3005 eV, respectively.

Molecular electrostatic potential (MEP)

The molecular electrostatic potential is related to electron density and has an important role for identifying sites for electrophilic attack and nucleophilic reactions[66,67]. It can also be used for describing many structural properties of the molecule such as chemical reactivity and dipole moment. The MEP of HL and $Cu^{II}(L)_2$ complex was calculated at the B3LYP/6-31G (d,p) level. The total electron density mapped with the electrostatic potential surface

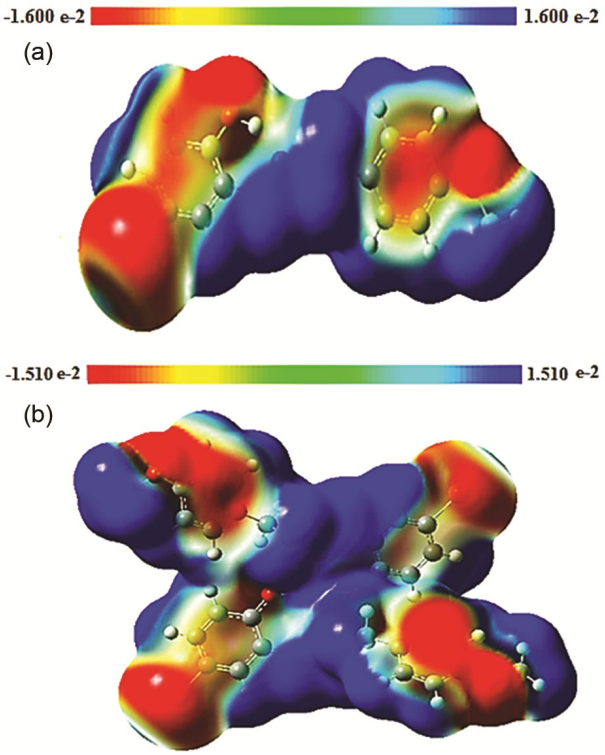

Fig. 4 — Molecular electrostatic potential maps of (a) HL and (b)$Cu^{II}(L)_2$at the B3LYP/6–31G(d,p) level of theory

is presented in Fig. 4. The colour scheme for the MEP surface is red (negative potential) and blue (positive potential). The MEP clearly indicates that the electron rich centres are found around the oxygen and the nitrogen atoms. However, positive electrostatic potential regions are localized on the hydrogen atoms. Thus, it can be predicted that an electrophile would preferentially attack HLon the O31 and N24 positions.

Atomic charges distribution

The Mulliken atomic charges of HL and its $Cu^{II}(L)_2$ complex, calculated using the DFT/B3LYP method, were illustrated in Table S3. For HL, the C21 atom has the largest Mulliken negative charge of -0.324673e among the carbon atoms. The high negative charge at C21 is due to the effect of the three positive atoms attached with it: C22, H25 and C6 with electron density of 0.280514e, 0.240134e and 0.055095e, respectively. On the other hand, it is observed that the most nucleophilic centers of HL are O19 and N24 atoms which is the most electrophilic susceptibility positions. The O19 atom attached with C12 and H20 atoms have -0.548725e atomic charge. Besides, the charges of O19 and N24 atoms have -0.573720e and -0.265577e, respectively. All H atoms have a positive charge ranged from 0.115258e (H29 atom) to 0.248372e (H26 atom).

SEM and EDX surface analysis

Fig. S7 shows scanning electron microscopy (SEM) and X-ray energy-dispersive analysis (EDX) spectra of HL and $Cu^{II}(L)_2$ complex. The surface images morphology of HL exhibits flower-like structures covering several forms of particles with a micron diameter size. The change in morphology of the $Cu^{II}(L)_2$ copper complex when compared to HL surface that appears as different, suggesting the formation of this novel complex. On the other hand, the chemical composition determined with energy dispersive X-ray (EDX) spectra confirms also the coordination. This corroborates with the presence of Cu(II) with two signals appearing at 0.9 and 8.05 KeV, respectively. Besides, the peaks of essential elements like carbon, nitrogen, oxygen and bromo signals, at ~0.27, ~0.39, ~0.52 and 1.5 KeV, respectively have been also observed. These data were undoubtedly indicative for the identification and characterization for molecular the structures of these both synthesized compounds[68]. So, the composition of HL and its copper complex with their experimental values are shown in Table S4.

Electrochemical properties

The electrochemical behaviour of $Cu^{II}(L)_2$ was studied by using cyclic voltammetry method in DMSO window with the potential range +1.50 to – 2.20 V (scan rate of 100 mV s^{-1}) and 0.1 M tetrabutylammonium perchlorate as supporting electrolyte. The cyclic voltammogram (Fig. S8a) displays two metal-centered quasi-reversible responses, one in the cathodic region, due to the Cu(II)/Cu(I) couple and the second in the anodic region, due to the Cu(III)/Cu(II) couple. The reduction response corresponding to Cu(II)/Cu(I) is observed at the half potential $E_{1/2}$ equal to – 0.89 V and with peak to peak separation of 0.18 V. As for the Cu(III)/Cu(II) process, it is observed at $E_{1/2}$ equal to +0.27 V with peak-to-peak separation of 0.28V. The ratio of cathodic to anodic peak height is less than the unity, 0.84 and 0.95 for Cu(II)/Cu(I) and Cu(III)/Cu(II), respectively. In addition, this complex shows Schiff base ligand oxidation response at about $E_{1/2}$ = 0.86 V and with peak-to-peak separation of 0.22 V. Finally, the reduction wave at – 1.75 V seems to be irreversible and may be ascribed to the reduction of azomethine function. The irreversibility of this redox process can be attributed to the instability of the reduced species in DMSO as used solvent.

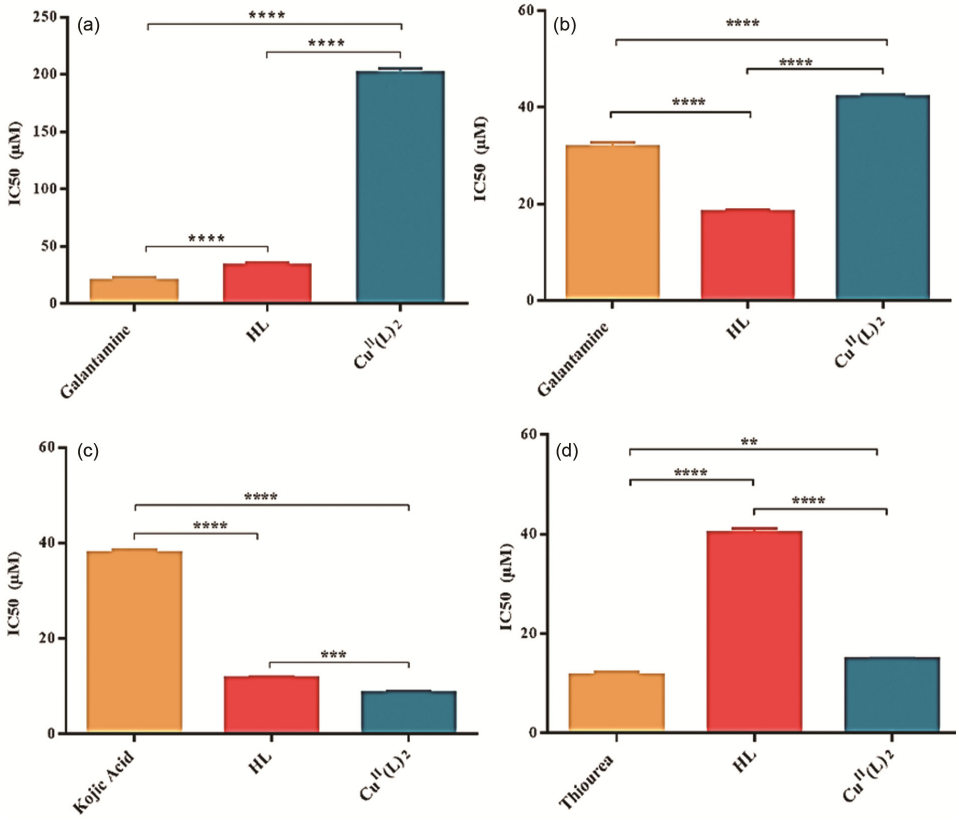

Fig. 5 — *In vitro* IC_{50} of the HL and $Cu^{II}(L)_2$ complex on (a) AchE, (b) BchE, (c) tyrosinase and (d) urease enzymatic methods

The influence of the scan rate recorded shows that the Ip increased with increasing scan rate. Moreover, the oxidation and reduction signals significantly shift to the more positive and negative potentials with the increasing of the scan rates. As well, the clearest indication that the process is not entirely reversible is the peaks separation of these systems which are significantly higher than 59 mV (100 mV<ΔEp<360 mV) and these values augment with the increase of scan rates. For the both systems Cu(II)/Cu(I) (Fig. S8b**)** and Cu(III)/Cu(II) **(**Fig. S8c**)**, the graph of Ipc and Ipa against square route of voltage $v^{1/2}$ gives a good linear relationship within scan rate in the range from 10 to 500 mVs^{-1}, involving a R^2 greater than 0.98. All these points established and confirmed that the electrode process could be compatible with a quasi-reversible implicating one-electron transfer, controlled by diffusion process. This result may probably be explained by the slow electron transfer or by an eventual adsorption of the electroactive species on the electrode surface. These results seem to be in agreement with those observed in the related Cu(II) complexes[45].

Powder X-ray diffraction

X-ray powder diffraction pattern is an important complementary technique usually used to look over and to identify the crystalline structure of materials. This method was used to get evidence about the structure of the prepared compounds. As shown in Fig. S9, XRD pattern of HL and $Cu^{II}(L)_2$ were recorded in the range (2θ= 4–90). The graph of copper complex is completely dissimilar from that of the starting ligand, indicating the formation of copper coordination complexand both are highly crystalline[69].

Enzymatic inhibitory activities

The essential objective of this section is to contribute to the identification of new enzymes inhibitors such as tyrosinase; acetylcholinesterase, butyrylcholinesterase and urease *in vitro* and *in silico* using molecular docking.

***In vitro* inhibition assays**

By using spectrophotometric methods, HL and $Cu^{II}(L)_2$ complex were also tested for some enzymatic inhibition activities (cholinesterase, tyrosinase and urease). The enzyme inhibition (%) and IC_{50} values are calculated and represented in Fig. 5 and Table 8.

Table 8 — Percentage enzyme inhibition and IC_{50} values

Sample	*In vitro* enzymatic inhibitory activities			
	Anticholinesterase		Tyrosinase IC_{50} (μM)	Urease IC_{50} (μM)
	Ach Eassay IC_{50} (μM)	BchE assay IC_{50} (μM)		
HL	35.3 ± 0.75	18.4±0.45	11.72 ± 0.28	40.17±0.98
$Cu^{II}(L)_2$	> 200	42.12±0.56	8.58 ± 0.45	14.81±0.28
Galantamine	21.82 ± 4.00	31.77 ± 0.14	N.T	N.T
Kojic Acid	N.T	N.T	37.86±0.78	N.T
Thiourea	N.T	N.T	N.T	11.57±0.68
Quercetin	N.T	N.T	N.T	N.T

Table 9 — Docking scores obtained from molecular docking analysis

Sample	Binding Affinity (kcal/mol)			
	4EY7	4TPK	2Y9X	1E9Z
HL	-6.8	-6.0	-6.9	-7.1
$Cu^{II}(L)_2$	-9.3	-10.3	-9.4	-10.8

Anticholinesterase activity

Regarding the enzymatic inhibition will allow to estimate the capacity of HL and its $Cu^{II}(L)_2$ copper complex against the anticholinesterase activity. Therefore, these compounds were evaluated using AchE and BchE enzymes. As it can be seen in Table 8, the active compound able of inhibiting AchE is HL (IC_{50} = 35.3 ± 0.75μM) which is adjacent to galantamine (IC_{50}= 21.82 ± 4.00 μM) that it is adopted as standard. As for copper complex, very slight inhibitory effect on this enzyme was observed with IC_{50}> 200 μM. The obtained IC_{50} values revealed that the HL compound shows a potent inhibition (IC_{50} = 18.4±0.45 μM), which is better than the standard BchE enzyme inhibitors Galantamine (IC_{50} =31.77 ± 0.14 μM) followed by $Cu^{II}(L)_2$ with an (IC_{50} = 42.12±0.56 μM), which is close to that of standard.

Tyrosinase inhibitory activity

The inhibitory effect of HL and$Cu^{II}(L)_2$towards tyrosinase activity is presented in Fig. 5 and Table 8. It can be seen that the better tyrosinase inhibitory activity is shown for both compounds HL and $Cu^{II}(L)_2$(IC_{50}=11.72 ± 0.28, 8.58 ± 0.45 μM, respectively) compared to Kojic acid used as control for this activity (IC_{50}=37.86±0.78 μM). After complexation with copper ion, an increase in the inhibitory activity is obviously noted with highest activity for this complex $Cu^{II}(L)_2$ higher than that of the used standard. So, it becomes clear that the presence of metal center improves significantly this activity.

Urease inhibitory activity

As shown in Table 8, the Schiff base ligand (IC_{50} = 40.17±0.98 μM) showed a good inhibition of the urease activity compared to Thiourea standard (IC_{50} = 11.57±0.68 μM). Now, it is clearly established that this inhibition increases significantly after coordination of an organic ligand with copper ion (IC_{50} = 14,81±0.28 μM) by giving an activity very close to the standard.

***In silico* molecular docking analysis**

The binding mode of the crystal structures ofthe four different proteinswith the two ligands was investigated through performing *in silico* analysis. It was shown that polar bonds play an important role in the affinity of the ligands towards the active sites of these proteins. Also, the hydrophobic surface of the ligands takes part in the optimization of interactions with the hydrophobic pocket of the proteins. The maximum binding scores obtained for the ligand-protein complex are given in Table 9. Also, the types of interactions betweendifferent amino acids and ligands are shown in the following Fig. 6.

To understand the potential anti-cholinesterase and anti-butyrylcholinesterase activity of HL, binding interactions between ligand and crystal structures (PDB: 4EY7) and (PDB: 4TPK), respectively, were analyzed and the results are shown in the below Fig. 6 (a and b).The potential inhibiting activity of HL against Helicobacter pylori urease (PDB ID: 2Y9X) andmushroom tyrosinase (PDB ID: 1E9Z) in the diagram displayed in Fig. 6 (c and d).

In Fig. 6a, HL forms strong interactions with acetylcholinesterase through the formation of conventional hydrogen bonds (green colour) with the side chains of His381 and Gln527 and strong π-Alkyl interaction with the Ala528. As for Fig. 6b, HL forms two strong hydrogen bonds with Pro230 and Ser287

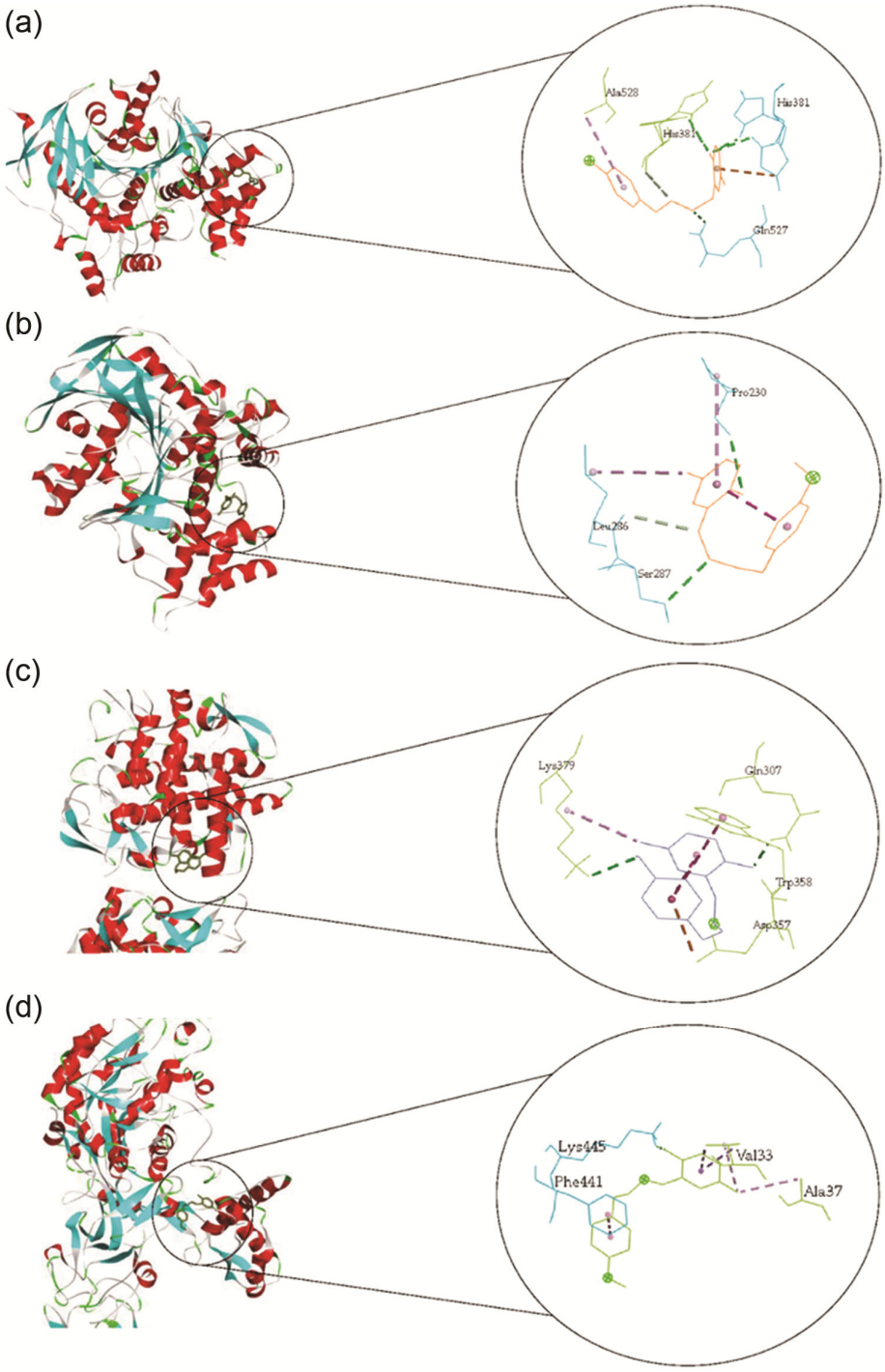

Fig. 6 — Docking poses of HL(a, b) against targeted cholinesterase and butyrylcholinesterase enzymes. Binding poses of HL with crystal structures (PDB ID: 2Y9X) and (PDB ID: 1E9Z) respectively (c,d).

of the butyrylcholinesterase enzyme. Also, its N atom exhibits a C-H bond with Leu286. Then, in Fig. 6c, HL inhibits urease through the formation of strong π-π bonds (purple colour) with Gln307 and Trp358 amino acids. Also, there is a π-anion interaction with the side chain of Asp357. In addition, two polar hydrogen form bonds with Lys379 and Gln307. Finally, in Fig. 6d, *in silico* evidence for the binding of HL to tyrosinase shows a conventional hydrogen bond with the side chain of Lys445, π-σ interaction

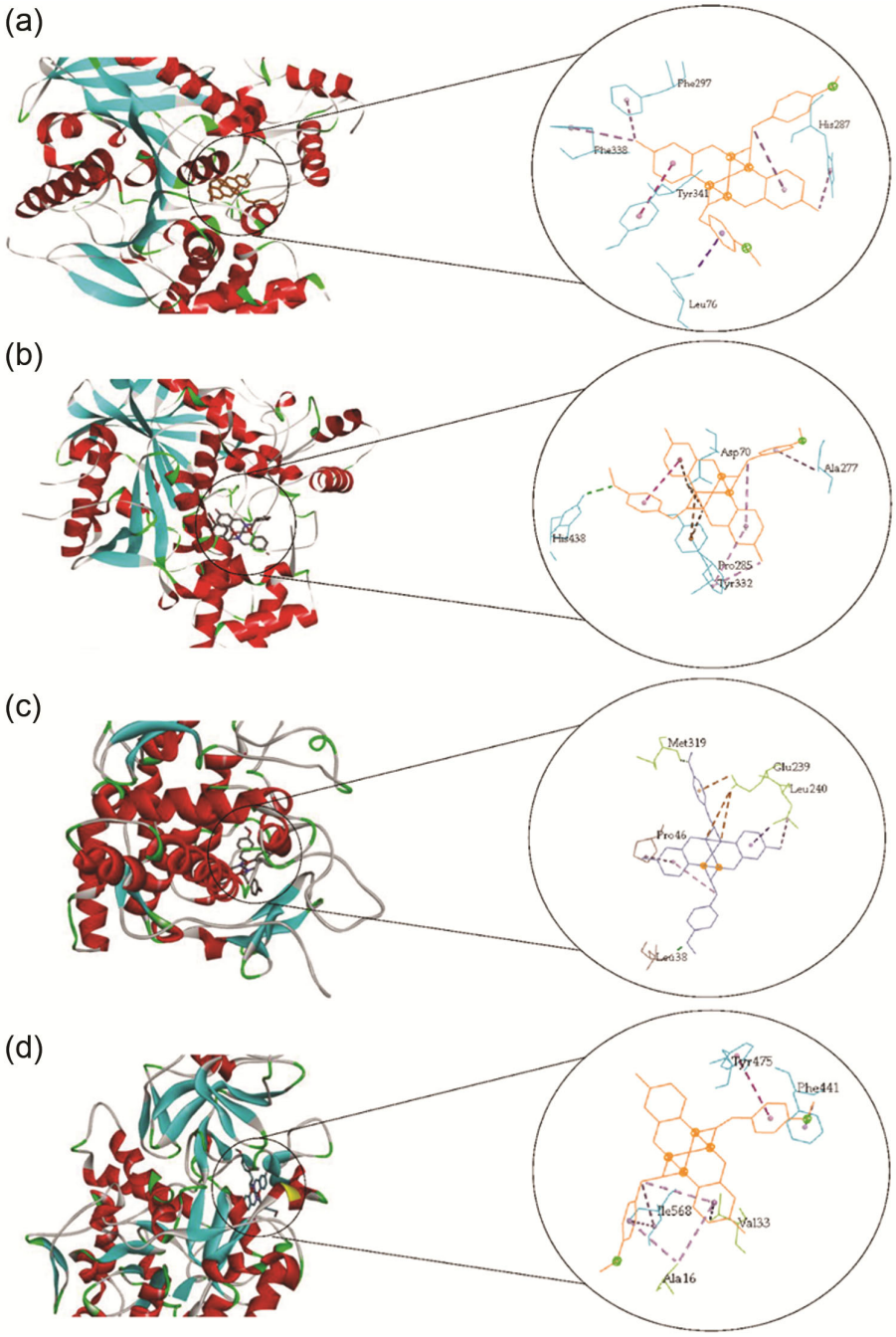

Fig. 7 — Effect of $Cu^{II}(L)_2$ as a promising inhibitor for (a) cholinesterase and (b) butyrylcholinesterase activity, (c) Anti-tyrosinase and (d) anti-urease activity of $Cu^{II}(L)_2$ against crystal structures (PDB: 2Y9X) and (1E9Z)

with the side chain of Val33, π-Alkyl interaction with Ala37, and π-π interaction with Phe441.

To recognize the promising anti-enzymatic activity of $Cu^{II}(L)_2$on the molecular level, *in silico* molecular docking studies were done. Fig. 7 (a, b) shows the different binding poses of $Cu^{II}(L)_2$within the active binding pocket of cholinesterase and butyryl-cholinesterase enzymes. The promising inhibitory activity of $Cu^{II}(L)_2$ towards tyrosinase and urease enzymes is showed in Fig. 7 (c, d).

As can be seen in Fig. 7a, *in silico* evidence for the binding of $Cu^{II}(L)_2$with crystal structures (PDB: 4EY7) show strong π-π interaction between $Cu^{II}(L)_2$and Tyr341. Also, there is a π-σ with Leu76. In addition, π-alkyl interaction with His287, Phe338, and Phe297. In Fig. 7b, $Cu^{II}(L)_2$ forms strong interactions through

the formation of a hydrogen bond with His438, π-Alkyl interaction with Ala277 and Pro285, π-cation and π-anion interactions with Asp70 and Tyr332, respectively. Then, in Fig. 7c, $Cu^{II}(L)_2$ forms two conventional hydrogen bonds with Leu38 and Met319. Also, π-σ and π-Alkyl interactions with Leu240 and Pro46 respectively. In addition, π-Anion interaction formed between the ligand and Glu239 through it is N atom, O atom, and aromatic ring. Finally, in Fig. 7d, π-π interaction between $Cu^{II}(L)_2$ and Tyr475. Also, there is a π-σ with Phe441 and Val33. In addition, there is π-Alkyl interaction with Ala16, and Ile568.

The enzymatic result seems to be of a great importance seeing that these compounds contain aromatic moieties electronically delocalized with methoxy groups considered as the main donors of electrons. The studied HL is considered as motivating acetylcholinesterase inhibitors and more advantageous for human health as can be confirmed by the obtained results[70]. Similarly, Masuda *et al.*[71] have been discussed this point since, they have noted that some tyrosinase inhibitors are endowed with good antioxidant activity. Inversely, it should also be logic that a good antioxidant might be as well good tyrosinase activity suggesting a relationship between antioxidant effect and tyrosinase inhibitory activity. The urease inhibition by HL is probably due to possible hydrogen bonding between the hydroxyl group (OH) present in the Schiff base and an amino acid residue as active site of the urease enzyme[72]. Â. de Fátima *et al* in their review paper assemble examples of the most anti-urease Schiff base ligands (0.23 μM <IC_{50}< 37.00 μM) and complexes (0.03 μM < IC_{50}< 100 μM)[73]. As for $Cu^{II}(L)_2$ complex (with $3d^9$ electronic configuration), it is more effective than HL and this potent inhibitory activity might be due to the strong Lewis acid properties of Cu^{2+} metal ion[73].

The results of docking analysis showed the compatibility of HL and $Cu^{II}(L)_2$with the binding pockets of the cholinesterase and BChE enzymes. The relatively low binding affinity (-6.8, -6.0 kcal/mol) and (-9.3, -10.3 kcal/mol) for HL and $Cu^{II}(L)_2$respectively suggests the activity of HL and $Cu^{II}(L)_2$ as enzymes inhibitors. To explore the key interactions of HL and $Cu^{II}(L)_2$ with tyrosinase and urease enzymes, we studied the binding pattern with the crystal structures of these enzymes. The docking models of HL and $Cu^{II}(L)_2$ with tyrosinase were verified by redocking the co-crystalized ligand using the same technique. The results of these docking models manifest the good accommodation of HL and $Cu^{II}(L)_2$ in the active site of the enzymes. The interaction of ligands with the critical amino acids within the binding pocket of the enzymes suggests its ability to modulate their action.

ADMET prediction

The most important and most difficult step in drug discovery and development is carrying out DMPK (Drug Metabolism and Pharmacokinetics) studies, often referred to as ADMET, the initiation of early absorption, distribution, metabolism, excretion and toxicity. Drug candidates should possess favourable ADME properties and ideally non-toxic. Therefore, the designed compounds were evaluated of their ADME profile, including physicochemical Properties, drug-likeness, and bioavailability using SwissADME. Drug-likeness was established from structural or physicochemical inspections of development compounds advanced enough to be considered oral drug-candidates. Based on the predicted results summarized in Table 10 and regarding to the physicochemical properties drug-likeness properties indicate that HL obeyed to Lipinski's, Ghose's, Veber's, Egan's and Muegge's rule. This compound assessing their flexibility as well as their surface area, with bioavailability score of 0.55 and consensus log Po/w of 3.77.Contrary to $Cu^{II}(L)_2$which obeyed only to Veber's rule and pass-through Lipinski's filter with one violation regarding molecular weights, with bioavailability score of 0.55 and consensus log Po/w of 4.11.

For oral bioavailability, six important properties (i.e., lipophilicity, size, polarity, solubility, flexibility, and saturation) should be taken into account[40]. Our bioavailability radar plots showed that HL was in the optimal range for all physicochemical properties (lipophilicity: − 0.7 < XLOGP3 (3.96)< 5.0, size: 150 g/mol < MW (332.19)< 500 g/ mol, polarity: 20 $Å^2$< TPSA (41.82)< 130 $Å^2$, solubility: -6< Log S (ESOL) (-4.57)<0, flexibility: 0 < Num. of rotatable bonds (4) < 9)) with the exception of saturation: 0.25 < Fraction Csp3 (0.06) < 1, HL was moderately unsaturated, suggesting that the molecule has to fall entirely the pink area and therefore exhibiting good drug-likeness properties and orally bioavailable. $Cu^{II}(L)_2$was in the optimal range for two physicochemical properties only (polarity: 20 $Å^2$< TPSA (61.64) < 130 $Å^2$and flexibility: 0 < Num. of rotatable bonds (6) < 9)). It is predicted not orally bioavailable.

The main ADME parameters of the pharmacokinetic behavior of HL and $Cu^{II}(L)_2$ complex are described in Table 10. Gastrointestinal absorption and brain access are crucial to make an estimation. According to the Brain or

Table 10 — Physicochemical properties, drug-likeness, bioavailability, pharmacokinetics and toxicity parameters of HL and its copper complex $Cu^{II}(L)_2$

Physicochemical properties			Drug-likeness			Bioavailability (Radar Plot)	
Parameters	HL $C_{16}H_{16}NO_2Br$	$Cu^{II}(L)_2$ $C_{32}H_{30}N_2O_4Br_2Cu$	Rules	HL $C_{16}H_{16}NO_2Br$	$Cu^{II}(L)_2$ $C_{32}H_{30}N_2O_4Br_2Cu$	HL $C_{16}H_{16}NO_2Br$	$Cu^{II}(L)_2$ $C_{32}H_{30}N_2O_4Br_2Cu$
Molecular weight (g/mol)	332.19 g/mol	725.91 g/mol	Lipinski	Yes; 0 violation	Yes; 1 violation: MW>500		
Num. heavy atoms	20	41	Ghose	Yes	No; 3 violations: MW>480, WLOGP>5.6, MR>130		
Num. arom. Heavy atoms	12	24	Veber	Yes	Yes		
Fraction Csp3	0.06	0.12	Egan	Yes	No; 1 violation: WLOGP>5.88		
Num. rotatable bonds	4	6	Muegge	Yes	No; 2 violations: MW>600, XLOGP3>5		
Num. H-bond acceptors	3	4	Bioavailability score	0.55	0.55		
Num. H-bond donors	1	0	Consensus log Po/w	3.77	4.11		
Molar refractivity	85.73	175.32					
TPSA (Å2)	41.82 Å²	61.64 Å²					

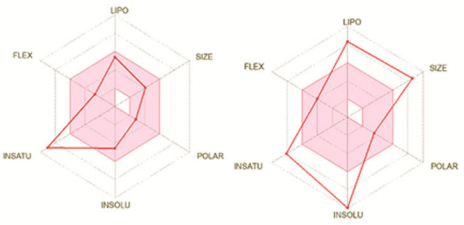

LIPO: Lipophilicity
FLEX: Flexibility
SIZE: Size

INSAT: Insaturation
INSOLU: Insolubility
POLAR: Polarity

Pharmacokenetics								
	HL $C_{16}H_{16}NO_2Br$	$Cu^{II}(L)_2$ $C_{32}H_{30}N_2O_4Br_2Cu$		HL $C_{16}H_{16}NO_2Br$	$Cu^{II}(L)_2$ $C_{32}H_{30}N_2O_4Br_2Cu$		HL $C_{16}H_{16}NO_2Br$	$Cu^{II}(L)_2$ $C_{32}H_{30}N_2O_4Br_2Cu$
GI absorption	High	Low	CYP1A2 inhibitor	Yes	No	CYP2D6 inhibitor	Yes	No
BBB permeant	Yes	No	CYP2C19 inhibitor	Yes	No	CYP3A4 inhibitor	Yes	No
P-gp substrate	No	Yes	CYP2C9 inhibitor	Yes	Yes	log Kp (skin permeation) cm/s	-5.51 cm/s	-4.25 cm/s

Toxicity								
AMES		hERG I inhibitor		Hepatotoxicity		Skin sensitisation		
HL $C_{16}H_{16}NO_2Br$	$Cu^{II}(L)_2$ $C_{32}H_{30}N_2O_4Br_2Cu$	HL $C_{16}H_{16}NO_2Br$	$Cu^{II}(L)_2$ $C_{32}H_{30}N_2O_4Br_2Cu$	HL $C_{16}H_{16}NO_2Br$	$Cu^{II}(L)_2$ $C_{32}H_{30}N_2O_4Br_2Cu$	HL $C_{16}H_{16}NO_2Br$	$Cu^{II}(L)_2$ $C_{32}H_{30}N_2O_4Br_2Cu$	
No	No	No	No	No	No	No	No	

Intestinal Estimated permeation method (BOILED-Egg) (Fig. 8**)**, HL was permeators of the blood brain barrier with high gastrointestinal absorption meaning their high absorbance potential which is a highly favourable feature of a drug candidate. These results demonstrating that HL was very likely to be passively absorbed by the gastrointestinal tract, contrary to $Cu^{II}(L)_2$.The BOLIED-Egg also showed that HL is not a P-gp substrate means there would not be an issue in the excretion of drug. P-glycoprotein plays a significant role in drug absorption and disposition. Because of its localization, P-glycoprotein appears to have a greater impact on limiting cellular uptake of drugs from blood circulation into brain and from intestinal lumen into epithelial cells than on enhancing the excretion of drugs out of hepatocytes and renal tubules into the adjacent luminal space[74]. On the contrary, the computational data for the $Cu^{II}(L)_2$ indicate it actively effluxed by P-gp (PGP+). It is well known that cytochrome P450s are important proteins relevant to pharmacokinetics which regulate the metabolism of various drugs, these enzymes are important for detoxification and they are present in all tissues of the body[75].

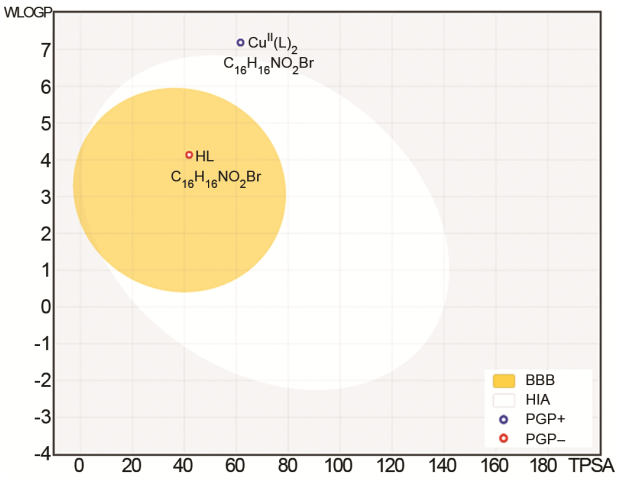

Fig.8 — The BOILED-Egg allows for intuitive evaluation of passive gastrointestinal absorption (HIA) and brain penetration (BBB) in function of the position of HL and its copper complex $Cu^{II}(L)_2$ in the WLOGP-*versus*-TPSA referential

Frequently, phase I metabolism reactions do not determine a substantial modification in the molecular weight or aqueous solubility of the substrate. At this stage, functional polar groups, such as hydroxyl (–OH*)*,

Sulfhydryl (–SH) or amino(–NH_2), are introduced into the parent molecule, thus rendering it nearby to further metabolism[76]. CYP monooxygenases play a key role in drug pharmacokinetics. They are commonly involved in drug–drug interactions. In human, fifty-seven CYP isoforms have been identified and among them, 12 metabolize 90% of xenobiotics and 6 CYP isoenzymes are able to metabolize the most common drugs used in therapy, respectively named CYP3A4, CYP3A5, CYP2D6, CYP2C9, CYP2C19 and CYP1A2 (Ref.77).

In this study, five major CYP isoforms (CYP1A2, CYP2C19, CYP2C9, CYP2D6 and CYP3A4) were considered during *in silico* prediction. As shown in Table 10, HL was found to be inhibitor of all cytochrome P450 isoforms CYP1A2, CYP2C19, CYP2C9, CYP2D6 and CYP3A4 which are the main players in Phase I metabolism. On the contrary, $Cu^{II}(L)_2$was found to be CYP2C9 inhibitor and no inhibitor of all cytochrome P450 isoforms. The CYP2C9 enzyme plays a major role in breaking down the anticlotting drug warfarin and assists in metabolizing the anti-inflammation drug ibuprofen[78]. Consequently, $Cu^{II}(L)_2$ may help to strengthen the effect of warfarin and ibuprofen. CYPs are often upregulated by their own substrates, leading to improved metabolism and plasma concentrations of the synchronized drugs. On the contrary, CYP inhibition by HL delivers high therapeutic HL levels and HL -induced toxicity, preventing CYPs from fulfilling their protective role in detoxification. The influence of CYPs on HL toxicity may be mainly exerted by either reducing the exposure to the parent compound or by transforming the HL Schiff base into a toxic compound. Furthermore, interindividual variability in CYP-mediated drug metabolism may exist, with some isoforms, including CYP1A2, CYP2B6, CYP2C8, CYP2C9, CYP2C19, CYP2D6 and CYP3A4/5, being extremely polymorphic[79].

Both HL and its copper complex $Cu^{II}(L)_2$ exhibited negative results on Ames mutagenesis and therefore cannot be considered as a mutagenic agent. In addition, no toxicity was shown with the human ether-a-go-gorelated gene (hERG I) inhibitor, and no hepatotoxicity and skin sensitization, which allows them to be good safety drugs. Considering that molecular weight, WLOGP, XLOGP3, influence permeability. In this context, the low oral bioavailability of $Cu^{II}(L)_2$ could be explained in terms of their calculated parameters according to Drug-like's rule. Thus, these compounds are predicted to be hardly transported, diffused, and absorbed than compared with the small molecules. On the other hand, many drugs that do not pass through the Lipinski's filter but have immense pharmacological properties have been approved by the FDA as potential drug for clinical purposes. Despite violation of some rules, approved anticancer and anti-infective drugs from natural products or their semisynthetic derivatives such as taxol and amphotericin B have also some violations but are biologically effective as drugs[80]. Therefore, these results do not interfere with the development of these compounds as potential therapeutic agents against acetylcholinesterase, butyrylcholinesterase, tyrosinase, and urease.

Conclusion

In this study, the synthesis and various characterization methods were fully reported for a novel synthesized bidentate ligand named 5-bromo-2-[(4-methoxyethyl phenyl)iminomethyl]phenol with its copper(II) complex. The resulting structures were confirmed by elemental analyses, NMR, IR, UV-visible, mass spectral and X-ray crystallographic analysis. The thermal properties and powder morphologies of the both studied samples using TG/DTG, SEM, EDX and powder XRD analysis that showed that the particles matched well with proposed elemental compositions. The electrochemical investigation of Cu(II) complex shows quasi-reversible redox properties of two systems Cu(III)/Cu(II)and Cu(II)/Cu(I). Then, among the analyzed enzymatic methods, the prepared compounds were proved as potent tyrosinase inhibition activity *in vitro* and *in silico*. From the perspective of this study, the obtained results indicate that other necessary tests should be carried out with these compounds such as antioxidant, antibacterial agent, including the mechanism with which the action of these compounds could be elucidated. Finally, more studies are also needed to evaluate the *in vivo* potential of these compounds in animal models.

Acknowledgements

The authors thank the Algerian Ministry of Higher Education and Scientific Research (MESRS) and the Director General for Scientific Research and Technological Development (DGRSDT) for the financial support.

Supplementary Information

Supplementary information is available on the website http://nopr.niscpr.res.in/handle/123456789. CCDC reference number of HL is 2122811 and copy

of this information is free of charge through the Cambridge Crystallographic Data Centre, 12 Union Road, Cambridge CB2 1EZ, UK, Fax: (+44)-1223-336033/ Email: deposit@ccdc.cam.ac.u.

References

1 Pervez H, Ahmad M, Zaib S, Yaqub M, Naseer M M & Iqbal J, Synthesis, cytotoxic and urease inhibitory activities of some novel isatin-derived bis-Schiff bases and their copper(II) complexes, *Med Chem Commun*, 7 (2016) 914.

2 Shah S S, Shah D, Khan I, Ahmad S, Ali U & ur Rahman A, Synthesis and antioxidant activities of Schiff bases and their complexes: An updated review, *Bio-interface Res Appl Chem*, 10 (2020) 6936.

3 Creaven B S, Duff B & Egan D A, Anticancer and antifungal activity of copper(II) complexes of quinolin-2(1H)-one-derived Schiff bases, *Inorg Chim Acta*, 363 (2010) 4048.

4 Mandewale M, Thorat B & Yamgar R, Synthesis and anti-mycobacterium study of some fluorine containing Schiff bases of quinoline and their metal complexes, *Der Pharma Chem*, 7 (2015) 207.

5 Jarrahpour A, Khalili D, De C E, Salmi C & Brunel J M, Synthesis, antibacterial, antifungal and antiviral activity evaluation of some new bis-Schiff bases of Isatin and their derivatives, *Molecules*, 12 (2007) 1720.

6 Pontiki E, Hadjipavlou-Litina D & Chaviara A T, Evaluation of anti-inflammatory and antioxidant activities of copper(II) Schiff mono-base and copper(II) Schiff base coordination compounds of dien with heterocyclic aldehydes and 2-amino-5-methyl-thiazole, *J Enzym Inhib Med Chem*, 23 (2008) 1011.

7 Luisi G, Stefanucci A, Zengin G, Dimmito M P & Mollica A, Anti-oxidant and tyrosinase Inhibitory in vitro activity of amino acids and small peptides: New hints for the multifaceted treatment of neurologic and metabolic disfunctions, *Antioxidants*, 8 (2019) 7.

8 Videira I F D S, Moura D F L & Magina S, Mechanisms regulating melanogenesis, *Ann Bras Dermatol*, 88 (2013) 76.

9 Nithitanakool S, Pithayanukul P, Bavovada R & Saparpakorn P, Molecular docking studies and anti-tyrosinase activity of Thai mango seed kernel extract, *Molecules*, 14 (2009) 257.

10 Kamkaen N, Mulsri N & Treesak C, Screening of some tropical vegetables for antityrosinase activity, *Thai Pharm Heal Sci J*, 2 (2007) 15.

11 Ketata A, Neifar A, Mihoubi W, Pigeon P, Gouzi H, Mallet J M, Top S, Gupta G K, Jaouen G, Gargouri A & El Arbi M, The inhibition of tyrosinase by some aryl butenes: A desired activity or a side effect to avoid, *J Organomet Chem*, 848 (2017) 133.

12 Moodie L W K, Sepčić K, Turk T, Frangež R & Svenson J, cholinesterase inhibitors from marine organisms, *Nat Prod Rep*, 36 (2019)1053.

13 Rosenberg P B, Nowrangi M A & Lyketsos C G, Symptoms in Alzheimer's disease: What might be associated brain circuits, *Mol Asp Med*, 43 (2015) 25.

14 Shah M I A, Khan R, Arfan M, Wadood A & Ghufran M, Synthesis, in vitro urease inhibitory activity and molecular docking of 3,5-disubstituted thiadiazine-2-thiones, *J Heterocycl Chem*, 1 (2019) 56.

15 Gholivand K, Pooyan M, Mohammadpanah F, Pirastefar F, Junk P C, Wang J, Valmoozi A A E & Mani-Varnosfaderani A, Synthesis, crystal structure and biological evaluation of new phosphoramide derivatives as urease inhibitors using docking, QSAR and kinetic studies, *Bioorg Chem*, 86 (2019) 482.

16 Xu Y P, Qin J, Sun S M, Liu T T, Zhang X L, Qian S S & Zhu H L, Synthesis, crystal structures, molecular docking and urease inhibitory activity of nickel(II) complexes with 3-pyridinyl-4-amino-5-mercapto-1,2,4-triazole, *Inorg Chim Acta*, 423 (2014) 469.

17 Maghraoui N, Aggoun D, Bouzerafa B, Bezzi H, Ouennoughi Y, Lopez D, Garcıa M F, Ourari A & Mubarak M S, Synthesis, characterization, thermal stability, electrochemical behavior, and antioxidant activity of new oxovanadium(IV) and iron(II) tetradentate Schiff base complexes, *Arab J Chem*, 14 (2021) 103025.

18 (a) Messasma Z, Aggoun D, Houchi S, Ourari A, Ouennoughi Y, Keffous F & Mahdadi R, Biological activities, DFT calculations and docking of imines tetradentates ligands, derived from salicylaldehydic compounds as metallo-beta-lactamase inhibitors, *J Mol Struct*, 1228 (2021) 129463; (b) Aggoun D, Messasma Z, Bouzerafa B, Berenguer R, Morallon E, Ouennoughi Y & Ourari A, Synthesis, Characterization and DFT investigation of New Metal Complexes ofNi(II), Mn(II) and VO(IV) Containing N,O-donor Schiff Base Ligand, *J Mol Struct*, 1231 (2021) 129923.

19 (a) Ourari A, Bougossa I, Bouacida S, Aggoun D, Ruiz-Rosas R, Morallon E & Merazig H, Synthesis, characterization and X-ray crystal structure of novel nickel Schiff base complexes and investigation of their catalytic activity in the electrocatalytic reduction of alkyl and aryl halides, *J Iran Chem Soc*, 14 (2017) 703; (b) Messasma Z, Ourari A, Mahdadi R, Houchi S, Aggoun D, Kherbache A & Bentouhami E, Synthesis, spectral characterization, DFT computational studies and inhibitory activity of novel N_2S_2tetradentates Schiff bases on metallo-beta-lactamases of Acinetobacter baumannii, *J Mol Struct*, 1171 (2018) 672.

20 APEX-II ; Bruker AXS : Madison, WI, USA.

21 SAINT ; Bruker AXS : Madison, WI, USA.

22 SADABS ; Bruker AXS: Madison, WI, USA.

23 Burla M C, Caliandro R, Camalli M, Carrozzini G, Cascarano G L, De C L, Giacovazzo C, Polidori G & Spagna R, An improved tool for crystal structure determination and refinement, *J Appl Crystallogr*, 38 (2005) 381.

24 Sheldrick G M, SHELXT - Integrated space-group and crystal-structure determination, *Acta Cryst C*, 71 (2015) 3.

25 Farrugia L J, Win GX and ORTEP for Windows: an update, *J Appl Cryst*, 45 (2012) 849.

26 Macrae C F, Bruno I J, Chisholm J A, Edgington P R, McCabe P, Pidcock E, Rodriguez-Monge L, Taylor R, Van de Streek J & Wood P A, New features for the visualization and investigation of crystal structures, *J Appl Cryst*, 41 (2008) 466.

27 Hehre W J, Radom L, Schleyer P V R & Pople J A, Ab initio molecular orbital theory, Wiley, New York (1986).

28 Frisch M J, Trucks G W, Schlegel H B, Scuseria G E, Robb M A, Cheeseman J R, Scalmani G, Barone V, Mennucci B, Petersson G A, Nakatsuji H, Caricato M, Li X, Hratchian H P, Izmaylov A F, Bloino J, Zheng G, Sonnenberg J L, Hada

M, Ehara M, Toyota K, Fukuda R, Hasegawa J, Ishida M, Nakajima T, Honda Y, Kitao O, Nakai H, Vreven T, Montgomery J A J, Peralta J E, Ogliaro F, Bearpark M, Heyd J J, Brothers E, Kudin K N, Staroverov V N, Kobayashi R, Normand J, Raghavachari K, Rendell A, Burant J C, Iyengar S S, Tomasi J, Cossi M, Rega N, Millam J M, Klene M, Knox J E, Cross J B, Bakken V, Adamo C, Jaramillo J, Gomperts R, Stratmann R E, Yazyev O, Austin A J, Cammi R, Pomelli C, Ochterski J W, Martin R L, Morokuma K, Zakrzewski V G, Voth G A, Salvador P, Dannenberg J J, Dapprich S, Daniels A D, FarkasÖ, Foresman J B, Ortiz J V, Cioslowski J & Fox D J, Gaussian 09, Revision A.02, Gaussian, Inc., Wallingford CT (2009).

29 Dennington R, Keith T & Millam J, Gauss View Version 5, Semichem Inc, Shawnee Mission KS, 5 (2009).

30 Becke A D, Density-functional thermochemistry. III. The role of exact exchange, *J Chem Phys*, 98 (1993) 5648.

31 Ellman G L, Courtney K D, Andres V & Featherston R M, A new and rapid colorimetric determination of acetylcholiesterase activity, *Biochem Pharm*, 7 (1961) 88.

32 Chan E W C, Lim Y Y, Wong L F, Lianto F S, Wong S K, Lim K K, Joe C E & Lim T Y, Antioxidant and tyrosinase inhibition properties of leaves and rhizomes of ginger species, *Food Chem*, 109 (2008) 477.

33 Weatherburn M W, Phenol-hypochlorite reaction for determination of ammonia, *Anal Chem*, 39 (1967) 971.

34 https://discover.3ds.com/discovery-studio-visualizerdownload

35 Baskaran K P, Arumugam A, Kandasamy R & Alagarsamy S, *In silico* method for prediction of maximum binding affinity and ligand – protein interaction studies on alzheimer's disease, *Int J Res Granthaalayah*, 8 (2020) 362.

36 Gardelly M, Trimech B, Horchani S A, Znati M, Ben Jannet H & Romdhane A, Anti-tyrosinase and anti-butyry-lcholinesterase quinolines-based coumarin derivatives: Synthesis and insights from molecular docking studies, *Chem Afr*, 4 (2021) 491.

37 Mughal E U, Ashraf J, Hussein E M, Nazir Y, Alwuthaynani A S, Naeem N, Sadiq A, Alsantali R I & Ahmed S A, Synthesis and structural characterization of thioflavones and thioflavonols as potential tyrosinase inhibitors: in vitro and in silico studies, *ACS Omega*, 7 (2022) 17444.

38 Quy P T, Du L N H, Triet N T, Bui T Q, Hai N T T, Thang L Q, Cuong T D, Chen T V & Nhung N T A, In silico study on inhibitability of flavonoidal derivatives against Helicobacter pylori and their pharmacological potentiality, *Vietnam J Chem*, 60 (2022) 435.

39 Trott O & Olson A J, Auto Dock Vina: Improving the speed and accuracy of docking with a new scoring function, efficient optimization, and multithreading, *J Comput Chem*, 31 (2010) 455.

40 Daina A, Michielin O & Zoete V, Swiss ADME: A free web tool to evaluate pharmacokinetics, drug- likeness and medicinal chemistry friendliness of small molecules, *Nat Publ Gr*, 7 (2017) 1.

41 Daina A & Zoete V, A BOILED-Egg to Predict gastrointestinal absorption and brain penetration of small molecules, *Chem Med Chem*, 11 (2016) 1117.

42 Pires D E, Blundell T L & Ascher D B, pkCSM: Predicting small-molecule pharmacokinetic and toxicity properties using graph-based signatures, *J Med Chem*, 58 (2015) 4066.

43 (a) Al-amery M H A & Al-sahlanee T Q M, Synthesis, characterization, antioxidant and anticancer human studies of new metal ion complexes of poly Schiff base derived from 4-aminoacetophenone with 4-chloroaniline and salicylaldehyde, *Res J Chem Environ*, 23 (2019) 200; (b) Geary W J, The use of conductivity measurements in organic solvents for the characterization of coordination compounds, *Coord Chem Rev*, 7 (1971) 81.

44 Khalji A D & Das D, Studies on Co(II) and Cu(II) complexes of a ligand derived from 1,3- phenylenediamine and 5-bromosalicylaldehyde synthesis, characterization , thermal properties and use as new precursors for preparation cobalt and copper oxide nano-particles, *J Therm Anal Calorim*, 114 (2013) 671.

45 Ourari A, Aggoun D & Ouahab L, A novel copper(II)-Schif base complex containing pyrrole ring: synthesis, characterization and its modified electrodes applied in oxidation of aliphatic alcohols, *Inorg Chem Commun*, 33 (2013) 118.

46 Kursunlu A N, Guler E, Sevgi F & Ozkalp B, Synthesis, Spectroscopic characterization and antimicrobial studies of Co(II), Ni(II), Cu(II) and Zn(II) complexes with Schiff bases derived from 5-bromo-salicylaldehyde, *J Mol Struct*, 1048 (2013) 476.

47 Tyagi P, Chandra S, Saraswat B S & Yadav D, Design, spectral characterization, thermal, DFT studies and anticancer cell line activities of Co(II), Ni(II) and Cu(II) complexes of Schiff bases derived from 4-amino-5-(pyridin-4-yl)-4H-1,2,4-triazole-3-thiol, *Spectrochim Acta A*, 145 (2015) 155.

48 Dueke-Eze C U, FasinaT M & Mphahlele M J, Synthesis, characterization and solvent effects on the electronic absorption spectra of aminopyridine Schiff bases, *Asian J Chem*, 25 (2013) 8505.

49 Guo H, Jiang J, Shi Y, Wang Y, Liu J & Dong S, UV-Vis spectrophotometric titrations and vibrational spectroscopic characterization of meso-(p-hydroxyphenyl) porphyrins, *J Phys Chem B*, 108 (2004) 10185.

50 Figueras J, Hydrogen bonding, solvent polarity, and the visible spectrum of phenol blue and its derivativatives, *J Am Chem Soc*, 19 (1971) 3255.

51 Carreño A, Gacitúa M, Páez-Hernández D, Polanco R, Preite M, Fuentes J A, Mora G C, Chávez I & Arratia-Pérez R, Spectral, theoretical characterization and antifungal properties of two phenol derivatives Schiff base with an intramolecular hydrogen bond, *New J Chem*, 39 (2015) 7822.

52 Chaudhary N K & Mishra P, Metal complexes of a novel Schiff base based on penicillin: characterization, molecular modeling, and antibacterial activity study, *Bioinorg Chem Appl*, 2017 (2017) 6927675.

53 Jamain Z, Khairuddean M & Guan-Seng T, Liquid-crystal and fire-retardant properties of new hexa-substituted cyclotriphosphazene compounds with two Schiff base linking units, *Molecules*, 25 (2020) 2122.

54 Silverstein R M, Bassler G C & Morrill T C, Spectrometric identification of organic compounds, 4th Ed. Wiley, New York, (1981).

55 Ismail T M A, Saleh A A & El-Ghamry M A, Tetra- and hexadentate Schiff base ligands and their Ni(II), Cu(II) and Zn(II) complexes. Synthesis, spectral, magnetic and thermal studies, *Spectrochim Acta A*, 86 (2012) 276.

56 Liu L, Jia D Z, Ji Y L & Yu K B, Synthesis, structure and photo-chromic properties of 4-acyl pyrazolonederivants, *J Photochem Photobiol A*, 154 (2003) 117.

57 Arici C, Tahir M N, Ulku D & Atakol O, 4-Chloro-2-(4-oxo-pent-2-en-2-ylamino)phenol, *Acta Crystallogr C*, 55 (1999) 1691.

58 Jian F F, Zhao P S, Bai Z S & Zhang L, Quantum chemical calculation studies on 4-phenyl1-(propan-2-ylidene) thiosemicarbazide, *Struct Chem*, 16 (2005) 635.

59 Tarı G O, Ceylan Ü, Agar E & Eserci H, Crystal structure, spectroscopic investigations and quantum chemical computational study of 5-(diethylamino)-2-((3-nitrophenylimino) methyl) phenol, *J Mol Struct*, 1126 (2016) 83.

60 Srivastava R, Sinha L, Karabacak M, Prasad O, Pathak S K, Asiri A M & Cinar M, Spectral features, electric properties, NBO analysis and reactivity descriptors of 2-(2-Benzothiazolylthio)-Ethanol: Combined experimental and DFT studies, *Spectrochim Acta A*, 136 (2015) 1205.

61 Veselinović J B, Veselinović A M, Vitnik Ž J & NiKolić G M, Antioxidant properties of selected 4-phenyl hydroxycoumarins: Integrated in vitro and computational studies, *Chem Biol Interact*, 214 (2014) 49.

62 Fukui F, Yonezawa T, Nagata C & Shingu H, Molecular orbital theory of orientation inaromatic, heteroaromatic, and other conjugated molecules, *J Chem Phys*, 20 (1954) 1433.

63 Zhou Z & Parr R G, Activation hardness: new index for describing the orientation of electrophilic aromatic substitution, *J Am Chem Soc*, 112 (1990) 5720.

64 Perez P, Domingo L R, Aizman A & Contreras R, The electrophilicity index in organic chemistry, theoretical aspects of chemical reactivity, *Theoret Asp Chem React*, Elsevier, New York, NY, USA, (2007).

65 Domingo L R, Aurell M J, Perez P & Contreras R, Quantitative characterization of the global electrophilicity power of common diene/dienophile pairs in Diels-Alder reactions, *Tetrahedron*, 58 (2002) 4417.

66 Politzer P & Murray J S, Relationships between dissociation energies and electrostatic potentials of C-NO_2 bonds: applications to impact sensitivities, *J Mol Struct*, 376 (1996) 419.

67 Luque F J, Lopez J M & Orozco M, Perspective on electrostatic interactions of a solute with a continuum. A direct utilization of ab initio molecular potentials for the prevision of solvent effects, *Theor Chem Acc*, 103 (2000) 343.

68 Nagaveni V B, Mahadevan K M, Vijayakumar G R, Nagabhushana H, Naveen S & Lokanath N K, Synthesis, crystal structure and excellent photoluminescenceproperties of copper(II) and cobalt(II) complexes with Bis(1[(4-butylphenyl)imino]methyl naphthalen-2-ol) Schiff base, *J Sci Adv Mater Dev*, 3 (2018) 51.

69 Roy G B, Synthesis and study of physico-chemical properties of a new chiral Schiff base ligand and its metal complex, *Inorg Chim Acta*, 362 (2009) 1709.

70 Asgharia B, Zenginb G, Bahadoric M B, Abbas-Mohammadid M & Dinparaste L, Amylase, glucosidase, tyrosinase, and cholinesterases inhibitory, antioxidant effects, and GC-MS analysis of wild mint (Mentha longifolia var. calliantha) essential oil: A natural remedy, *Eur J Integr Med*, 22 (2018) 44.

71 Masuda T, Yamashita D, Takeda Y & Yonemori S, Screening for tyrosinase inhibitors among extracts of seashore plants and identification of potent inhibitors from Garcinia subelliptica, *Biosci Biotechnol Biochem*, 69 (2005) 197.

72 Rahim F, Shehzad M, Khan A, Taha M, Quereshi M T, TauseefI & Rehman W, Synthesis and antiurease & antioxidant activities of Bis-Schiff bases of isophthalaldehyde, *Asian J Chem*, 28 (2016) 39.

73 (a) Li Y G, Shi D H, Zhu H L, Yan H & Ng S W, Transition metal complexes (M = Cu, Ni and Mn) of Schiff-base ligands: syntheses, crystal structures, and inhibitory bioactivities against urease and xanthine oxidase, *Inorg Chim Acta*, 360 (2007) 2881; (b) de Fátima Â, de Paula Pereira C, Olímpio C R S D G, de Freitas Oliveira B G, Franco L L & da Silva P H C, Schiff bases and their metal complexes as urease inhibitors – A brief review, *J Adv Res*, 13 (2018) 113.

74 Mishra S & Dahima R, In-vitro ADME studies of TUG-891, a GPR-120 inhibitor using Swiss ADME Predictor, *J Drug Deliv Ther*, 9 (2019) 366.

75 Ouassaf M, Belaidi S, Khamouli S, Belaidi H & Chtita S, Combined 3D-QSAR and molecular docking analysis of Thienopyrimidinederivatives as Staphylococcus aureus inhibitors, *Acta Chim Slov*, 68 (2021) 289.

76 Iacopetta D, Ceramella J, Catalano A, Scali E, Scumaci D, Pellegrino M, Aquaro S, Saturnino C & Sinicropi M S, Impact of cytochrome P450 enzymes on the phase I metabolism of drugs, *Appl Sci*, 13 (2023) 6045.

77 Williams J A, Hyland R, Jones B C, Smith D A, Hurst S, Goosen T C, Peterkin V, Koup J R & Ball S E, Drug-drug interactions for UDP-glucuronosyltransferase substrates: a pharmacokinetic explanation for typically observed low exposure (AUCi/AUC) ratios, *Drug Metab Dispos*, 32 (2004) 1201.

78 NIH US *National Library of Medicine Genetics Home Reference*, Genes, CYP2C9 gene (2019).

79 Tracy T S, Chaudhry A S, Prasad B, Thummel K E, Schuetz E G, Zhong X B, Tien Y C, Jeong H, Pan X & Shireman L M, Interindividual variability in cytochrome P450–mediated drug metabolism, *Drug Metab Dispos*, 44 (2016) 343.

80 Houchi S & Messasma Z, Exploring the inhibitory potential of Saussurea costus and Saussurea involucrata phytoconstituents against the Spike glycoprotein receptor binding domain of SARS-CoV-2 Delta (B.1.617.2) variant and the main protease (Mpro) as therapeutic candidates, using Molecular docking, DFT, and ADME/Tox studies, *J Mol Struct*, 1263 (2022) 133032.